Open access • Journal Article • DOI:10.1016/J.EUROMECHFLU.2008.06.004

Current knowledge in hydraulic jumps and related phenomena: A survey of experimental results — Source link

Hubert Chanson

Institutions: University of Queensland

Published on: 01 Mar 2009 - European Journal of Mechanics B-fluids (Elsevier Masson)

Topics: Hydraulic jumps in rectangular channels, Hydraulic jump, Supercritical flow, Open-channel flow and Hydraulics

European Journal of Mechanics B/Fluids 28 (2009) 191–210

Contents lists available at ScienceDirect

European Journal of Mechanics B/Fluids

www.elsevier.com/locate/ejmflu

Current knowledge in hydraulic jumps and related phenomena. A survey of experimental results

Hubert Chanson [1]

Division of Civil Engineering, The University of Queensland, Brisbane QLD 4072, Australia

ARTICLE INFO

Article history:
Received 10 December 2007
Received in revised form 12 June 2008
Accepted 23 June 2008
Available online 1 July 2008

Keywords:
Hydraulic jumps
Undular hydraulic jumps
Positive surges
Tidal bores
Unsteady turbulence
Air bubble entrainment
Boussinesq equation
Two-phase flow properties
Dynamic similarity
Scale effects

ABSTRACT

The hydraulic jump is the sudden transition from a high-velocity open channel flow regime to a subcritical flow motion. The flow properties may be solved using continuity and momentum considerations. In this review paper, recent advances in turbulent hydraulic jumps are developed: the non-breaking undular hydraulic jump, the positive surge and tidal bore, and the air bubble entrainment in hydraulic jumps with roller. The review paper demonstrates that the hydraulic jump is a fascinating turbulent flow motion and the present knowledge is insufficient, especially at the scales of environmental and geophysical flows.

1. Introduction

Hydraulic jumps are commonly experienced in rivers and canals, in industrial applications and manufacturing processes, as well as in the kitchen sink. A hydraulic jump is the sudden transition from a supercritical open channel flow regime to a subcritical flow motion. For a horizontal rectangular channel and neglecting boundary friction, the continuity and momentum principles give [1]:

$$\frac{d_2}{d_1} = \frac{1}{2} \times \left(\sqrt{1 + 8 \times Fr_1^2} - 1\right) \quad (1)$$

$$\frac{Fr_2}{Fr_1} = \frac{2^{3/2}}{(\sqrt{1 + 8 \times Fr_1^2} - 1)^{3/2}} \quad (2)$$

where the subscripts 1 and 2 refer to the upstream and downstream flow conditions respectively, Fr is the Froude number: $Fr = V/\sqrt{g \times d}$, d and V are the flow depth and velocity respectively, and g is the gravity acceleration. The hydraulic jump is typically classified in terms of its inflow Froude number $Fr_1 = V_1/\sqrt{g \times d_1}$ that is always greater than unity [1,2]. For a Froude number slightly above unity, the hydraulic jump is characterised a smooth rise of the free-surface followed by a train of stationary free-surface undulations: i.e., the undular hydraulic jump (Fig. 1A). For larger Froude numbers, the jump is characterised by a marked roller, some highly turbulent motion with macro-scale vortices, significant kinetic energy dissipation and a bubbly two-phase flow region (Fig. 1B). The unsteady form of hydraulic jump is the positive surge that is also called a hydraulic jump in translation. A glossary of relevant terms is given at the end of the article.

Historically, significant contributions to the fluid dynamics of hydraulic jumps included the physical modelling of Bidone [11], the theoretical solution of the momentum principle by Bélanger [1], the experiments of Darcy and Bazin [10] (Fig. 2), the solutions of Boussinesq [12] and the work of Bakhmeteff [13] (see review in [14]). Although a laminar jump may occur for very-low inflow Reynolds number $Re = \rho \times V_1 \times d_1/\mu$ (e.g. [15]). most situations are turbulent flows. Fig. 1 presents two photographs of turbulent hydraulic jumps.

In this review, recent advances in turbulent hydraulic jumps are developed. It is the purpose of this contribution to show the complicated features of hydraulic jump flows commonly encountered in geophysical and environmental flows, and this is supported by relevant experimental evidences. The non-breaking undular hydraulic jump is discussed first. Then the case of the hydraulic jump

E-mail address: h.chanson@uq.edu.au.
URL: http://www.uq.edu.au/~e2hchans.

[1] The paper derives from a plenary lecture paper presented at the 16th Australasian Fluid Mechanics Conference [H. Chanson, Hydraulic jumps: Bubbles and bores. in: Proc. 16th Australasian Fluid Mechanics Conference AFMC, Gold Coast, Australia, 2–7 December, Plenary Address, 2007, pp. 39–53 (CD-ROM) [95]].

0997-7546/$ – see front matter
doi:10.1016/j.euromechflu.2008.06.004

(A)

(B)

Fig. 1. Photographs of hydraulic jump flows. (A) Undular hydraulic jump – flow conditions: $Fr_1 = 1.35$, $d_1 = 0.090$ m, $Re = 1.1 \times 10^5$ – flow from left to right. (B) Hydraulic jump with roller – flow conditions: $Fr_1 = 7.0$, $d_1 = 0.024$ m, $Re = 8.1 \times 10^4$ – flow from left to right.

Table 1
Summary of recent experimental studies of undular hydraulic jumps

	Channel	Instrumentation
Chanson and Montes [3]	$L = 20$ m, $B = 0.25$ m, F/D inflow	Prandtl–Pitot tube (∅3.3 mm)
Montes and Chanson [4]	$L = 12$ to 20 m, $B = 0.2$ to 0.3 m, F/D inflow	Prandtl–Pitot tubes
Chanson [5]	$L = 20$ m, $B = 0.25$ m, F/D inflow	Pitot–Preston tube (∅3.3 mm)
Ohtsu et al. [6]	$L = 5$ to 20 m, $B = 0.1$ to 0.8 m, P/D & F/D inflow	Micro-propeller (∅3 mm), Prandtl–Pitot tube, 1D-LDV
Chanson [7]	$L = 3.2$ m, $B = 0.5$ m, P/D inflow	Prandtl–Pitot tube (∅3.3 mm)
Lennon and Hill [8]	$L = 4.9$ m, $B = 0.3$ m, F/D inflow	Particle Image Velocimetry
Ben Meftah et al. [9]	$L = 15$ m, $B = 4$ m, F/D inflow	Acoustic Doppler Velocimetry

Notes. B: channel width; F/D: fully-developed; L: channel length, P/D: partially-developed.

in translation is considered: i.e., positive surges and tidal bores. The last section discusses the air bubble entrainment in hydraulic jumps with roller, its physical modelling, the dynamic similarities and scale effects.

2. Undular hydraulic jumps

Undular hydraulic jumps are characterised by a smooth rise of the free-surface followed by a train of well-formed stationary waves (Figs. 1A, 2B, 3). They are sometimes experienced in natural waterways and rivers at a break in bed slopes. A related situation is the "Morning Glory" cloud pattern observed in Northern Australia, sometimes called an undular jump [16,17].

Most hydraulic and fluid mechanics textbooks ignore the undular hydraulic jump in their section on open channel flows. A few studies of hydraulic jumps included some undular jump cases: e.g., Darcy and Bazin [10], Bakhmeteff and Matzke [18], Binnie and Orkney [19] (Fig. 2). Fawer [20] detailed clearly the main features of undular hydraulic jumps but his contribution was ignored for decades. Modern studies of undular jumps included Montes [21], Ryabenko [22], Chanson and Montes [3], Montes and Chanson [4], Ohtsu et al. [6]. These works showed that undular jumps may occur for upstream Froude numbers ranging from unity up to 3 to 4.

Recent experiments (Table 1) are re-analysed herein and the results provide some new understanding of the complicated flow patterns in undular hydraulic jumps.

2.1. Free-surface wave characteristics

Visual observations and detailed free-surface measurements showed that an undular jump is basically two-dimensional but next to the sidewalls (Fig. 3). The free-surface undulations are quasi-periodic, but the longitudinal profile is neither sinusoidal nor cnoidal. Fig. 3B presents the dimensionless free-surface profile for an experiment ($Fr_1 = 1.26$), where x is the distance measured

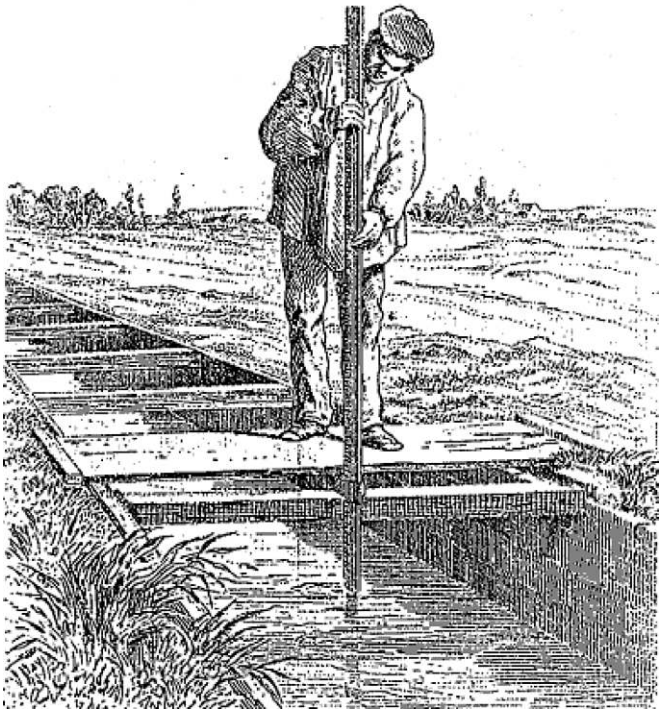

(A)

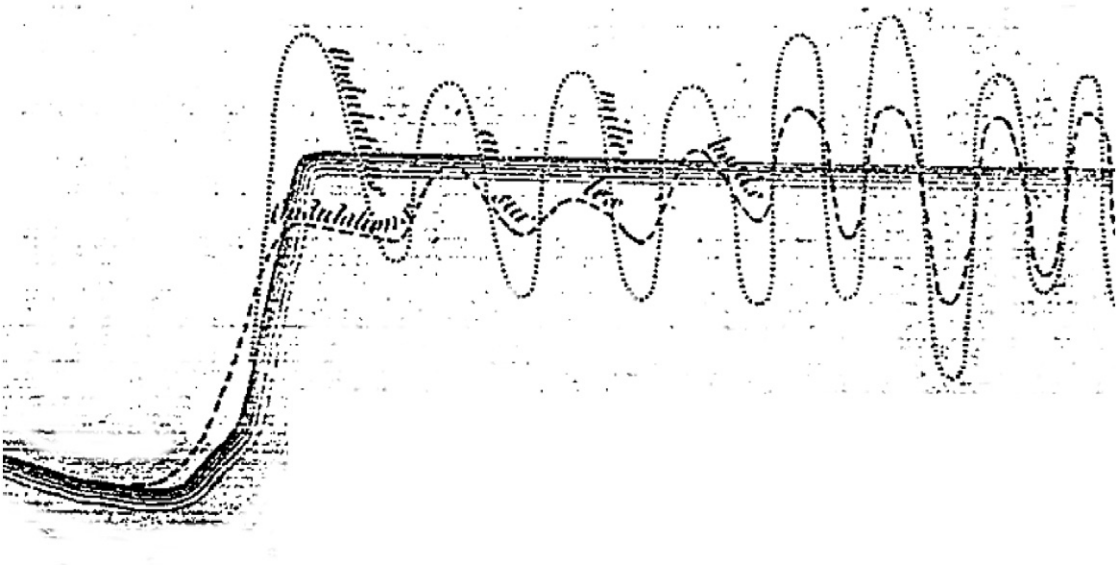

(B)

Fig. 2. Undular hydraulic jump experiments of Darcy and Bazin [10]. (A) Free-surface measurement technique. (B) Data on Pont-aqueduc de Crau, Canal de Craponne.

Table 2
Maximum wave amplitude $(a_w)_{max}/d_1$ of the first undulation and corresponding Froude number

d_c/B	$(a_w)_{max}/d_1$	$(Fr_1)_{max}$
0.14	0.64	1.68
0.17	0.46	1.58
0.22	0.42	1.51
0.225	0.34	1.47
0.28	0.27	1.39
0.35	0.23	1.275
0.40	0.18	1.30
0.46	0.18	1.275

Note. Undular jump data: Chanson [23].

from the upstream gate, d is the flow depth, d_c is the critical depth: $d_c = \sqrt[3]{Q^2/(g \times B^2)}$, Q is the discharge and B is the channel width. The free-surface measurements were conducted on the channel centreline ($z = 0$) and at three transverse locations. Sidewall cross waves were seen upstream of the first wave crest and sometimes immediately upstream of the downstream wave crests (Fig. 3A). The angle of the shock waves with the wall was relatively shallow as sketched in Fig. 3A. Typical undular jump wave characteristics are presented in Figs. 4 and 5. The data included the amplitude and length of the first undulation which were observed for a range of aspect ratio d_c/B (Fig. 4), and the flow Froude number at shock wave formation and the angle of lateral shock waves with the sidewall (Fig. 5).

The wave properties were functions of the inflow Froude number Fr_1 and relative aspect ratio d_c/B. For Froude numbers slightly above unity, the wave length and amplitude data followed closely a solution of the Boussinesq equation [25] (Figs. 4A and 4B). With

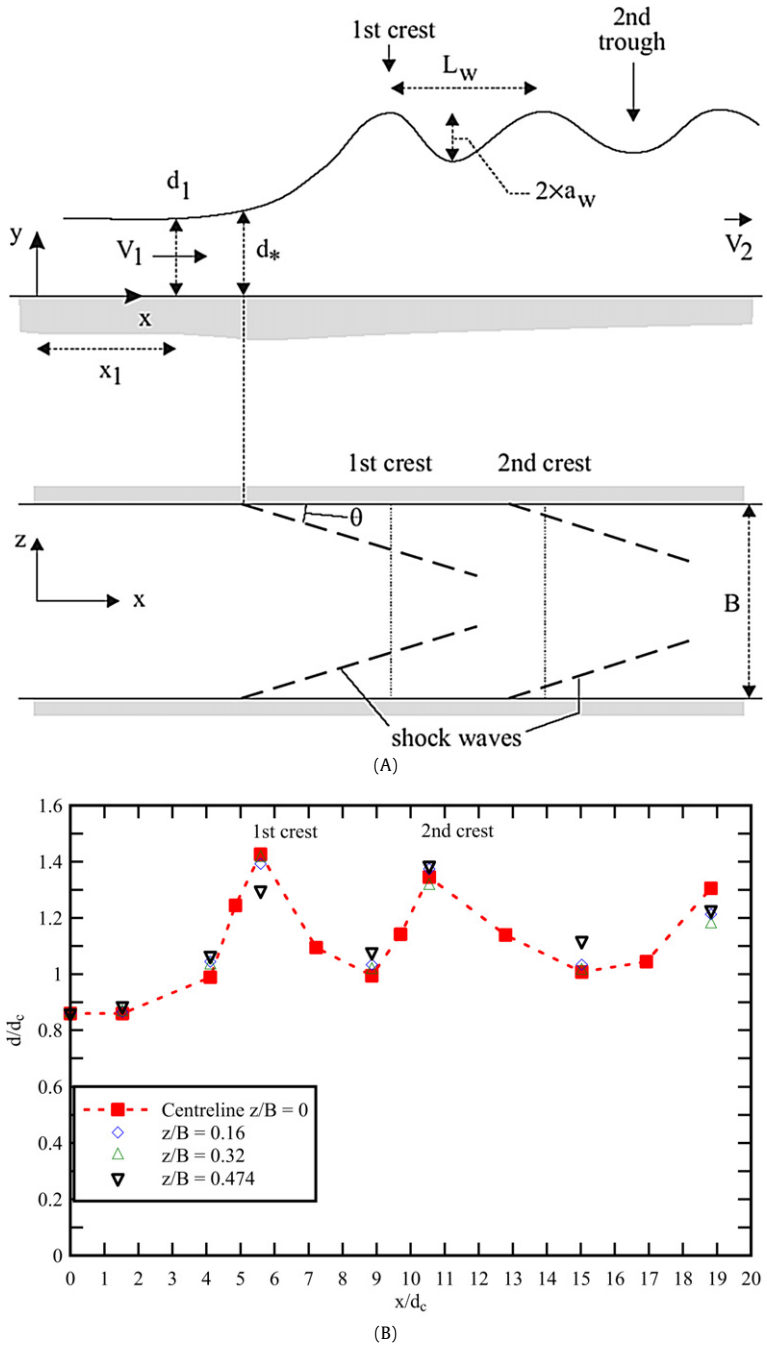

Fig. 3. Free-surface profile of an undular hydraulic jump. (A) Definition sketch. (B) Data: $Fr_1 = 1.26$, $d_1 = 0.082$ m, $Re = 9 \times 10^4$ [7].

increasing Froude numbers, both wave amplitude and wave length data diverged from the Boussinesq solution. The wave amplitude data showed a local maximum value for $Fr_1 = 1.3$ to 1.9 depending upon the aspect ratio (Fig. 4A). Maximum wave amplitude data are summarised in Table 2 for several aspect ratios and the corresponding inflow Froude number is listed. For the data sets shown in Fig. 4, the maximum wave amplitude was observed for $Fr_1 = 1.27$ to 1.7 and the disappearance of the free-surface undulations took place for $Fr_1 = 1.5$ to 3 (Fig. 3). The characteristic Froude number of undulation disappearance increased with increasing relative width and decreasing aspect ratio d_c/B. More generally, the free-surface undulations disappeared for $Fr_1 = 1.5$ to 4 with decreasing aspect ratio d_c/B, including recent experiments in Russia and Italy with 4.5 m and 4 m width channels respectively [9,22].

A major flow feature was the presence of lateral shock waves. The shock waves initiated upstream of the first wave crest and propagated downstream across the flume (Fig. 3A). Montes [21] suggested that the presence of lateral shock waves was connected with the sidewall boundary layers. He offered that the lateral boundary layers would retard the fluid near the wall and force the apparition of critical conditions sooner than on the channel centreline. Chanson [23] argued that the shock waves were a form of flow separation at the sidewalls, since flow recirculation was observed immediately downstream of the shock wave near the free-surface.

Some shock wave characteristics were recorded for a range of flow conditions. The data are reported in Fig. 5, where Fr_* and θ are plotted as functions of the upstream Froude number Fr_1. Fr_* is the flow Froude number at the inception of the shock waves:

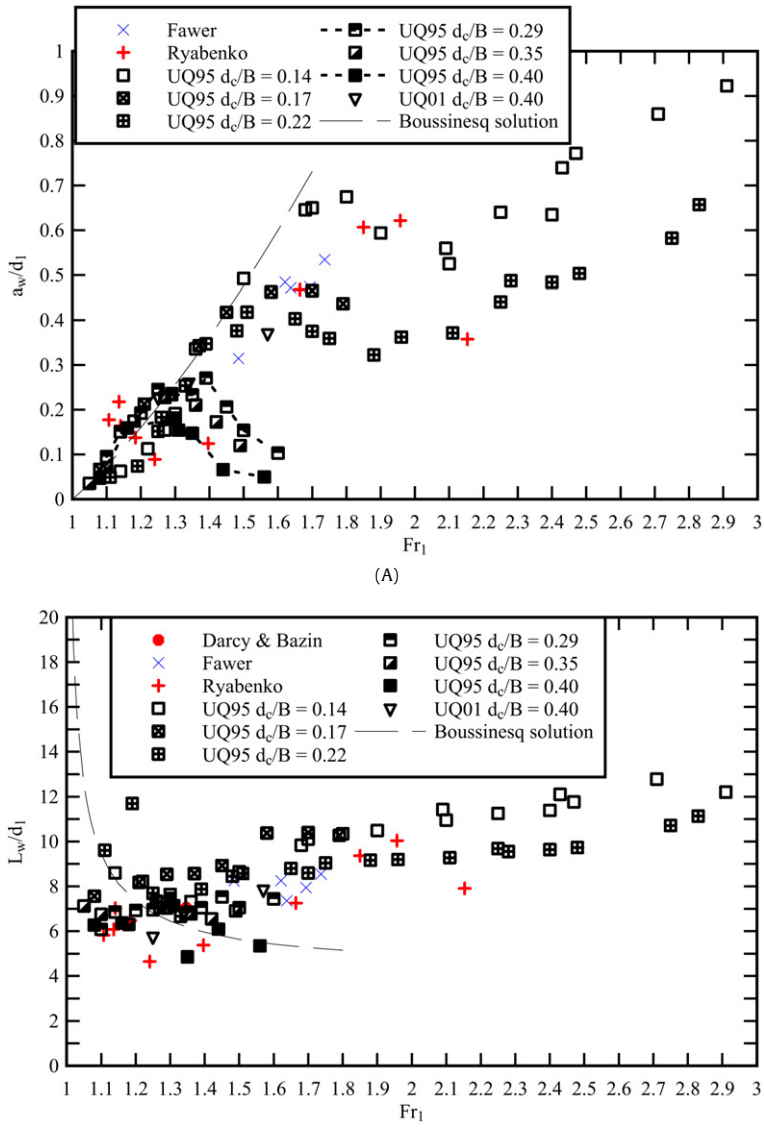

Fig. 4. Undular jump wave characteristics. Data: Darcy and Bazin [10], Fawer [20], Ryabenko [22], Chanson [23] [UQ95], Chanson [7] [UQ01]. (A) Dimensionless wave amplitude a_w/d_1. (B) Dimensionless wave length L_w/d_1.

$Fr_* = q/\sqrt{g \times d_*^3}$ and d_* is the flow depth at the onset of shock waves at the sidewall (Fig. 3A). The inception of the oblique jumps occurred in a region of supercritical flow which satisfied:

$$Fr_* = Fr_1 - 0.119 \quad (3)$$

Eq. (3) is compared with experimental data in Fig. 5A. The shock wave observations showed an increasing angle with the sidewall with increasing Froude number and the results were nearly independent of the aspect ratio. The data were best correlated by:

$$\theta = 28.1 \times Fr_1^{0.38} \quad (4)$$

Eq. (4) is compared with the data in Fig. 5B. The data were quantitatively close to shock wave calculations in supercritical flows [24,32], but the trend was opposite: i.e., in supercritical flows, the shock waves propagate above the high-velocity supercritical flow motion, and the angle θ decreases with increasing Froude number (Fig. 5B). In contrast, in an undular jump, the shock waves propagated above a subcritical flow.

2.2. Velocity and pressure distributions in undular jumps

Beneath the free-surface undulations, rapid redistributions of pressure and velocity fields were observed between crests and troughs. Fig. 6 presents typical dimensionless pressure and velocity distributions in an undular jump ($Fr_1 = 1.6$). In Fig. 6, the data are compared with an inviscid solution of the Boussinesq equation [4]. In the undular flow, the pressure distributions were not hydrostatic. The pressure gradients were larger than hydrostatic when the free-surface was curved upwards (i.e. concave) and less than hydrostatic when the free-surface was convex. The trend was predicted by the irrotational flow motion theory (e.g. [33,34]), although greater deviations from hydrostatic pressure distributions were experimentally observed (Fig. 6). At the first wave crest, the velocity distributions differed considerably from theoretical predictions (Fig. 6A). For that experiment, the flow was affected by some recirculation "bubble" beneath the first crest, described by Montes [21]. More generally, however, the flow was subjected to a major velocity redistribution immediately upstream of the first crest [3,7,8]. The flow field at the first wave tended to differ significantly

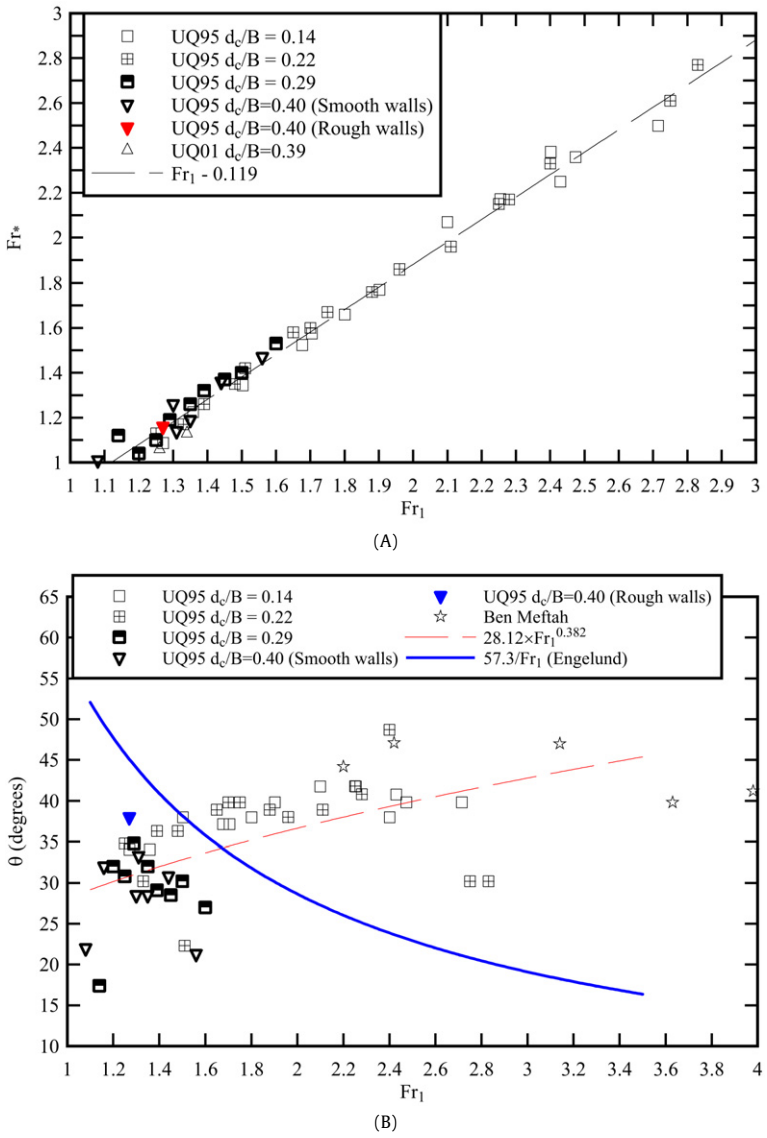

Fig. 5. Shock wave characteristics of undular hydraulic jumps. Data: Chanson [23] [UQ95], Chanson [7] [UQ01], Ben Meftah et al. [9]. (A) Flow Froude number Fr_* at the inception of the lateral shock waves with the sidewall – comparison with Eq. (3). (B) Angle θ of the lateral shock waves with the sidewall – comparison with supercritical flow results [24] (Eq. (4)).

from those at the subsequent wave crest. Further downstream, the agreement between data and theory improved (Fig. 6). The same trends were observed for a wide range of experiments (Table 1).

During an experiment, detailed velocity and pressure measurements were conducted on either side upstream and downstream of both crest and trough. The results showed consistently an absence of symmetry. There was no exact correspondence in shape and magnitude, on opposite sides of a crest or trough [7]. The velocity distribution data showed a greater flow acceleration next to the bottom (i.e. $y/d_c < 0.3$), between crest and trough, than the corresponding deceleration between trough and crest.

The experimental data suggested further that the flow region immediately upstream of the first wave crest was associated with some massive redistribution of the pressure and velocity fields. This flow region was characterised by some adverse pressure gradient, the initiation of the sidewall cross-waves and some substantial boundary layer development. For an observer travelling with the upstream flow, the region immediately upstream of the wave crest appeared to act as a "pseudo-wave maker" generating the downstream free-surface undulations.

2.3. Discussion

Some researchers used an analogy between undular jumps and surges advancing in still water and the various results were sometimes conflicting: e.g., Lemoine [35], Serre [36], Iwasa [37], Andersen [25]. Montes [38] argued first that the analogy between undular jump and undular surge does not take into account the true flow characteristics. In undular jumps, turbulent boundary layers are partially or fully developed along both the channel bed and the sidewalls. The undular jump extends over a great length, and the assumption of negligible bottom and sidewall friction is unrealistic.

Montes [21] and Ryabenko [22] developed two pertinent and independent studies. Their results refuted the analogy between undular jump and undular surge. Further, they suggested that the transition between an undular jump and a weak jump may occur for upstream Froude numbers in the range 1.0 to 3.6, the transition being a function of the upstream flow conditions, aspect ratio and bed roughness. In contrast, an undular surge disappears for surge Froude number greater than 1.5 to 1.8 [2,29,30,33]. Henderson [2], Rajaratnam [39], Leutheusser and Schiller [40]

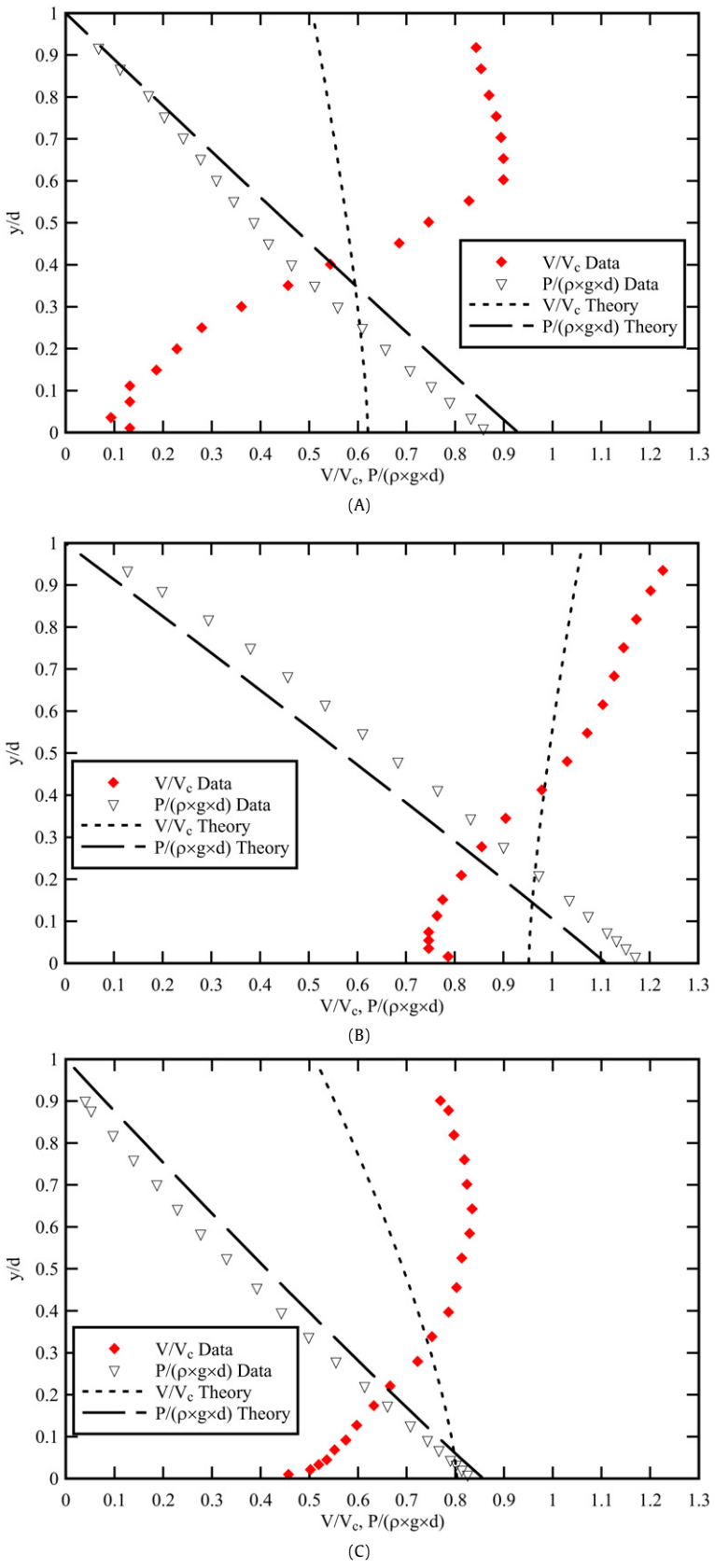

Fig. 6. Dimensionless pressure and velocity distributions in an undular jump: $Fr_1 = 1.57$, $Re = 1.1 \times 10^5$, Data: Chanson [7] – comparison with an inviscid solution of the Boussinesq equation. (A) First wave crest, (B) first trough, (C) second wave crest.

and Chanson [5] discussed the role of bottom and sidewall roughness on the undular jump flow. The experiments of Henderson [2] and Leutheusser and Schiller [40] suggested that undular flows above a rough bed take place for a wider range of Froude numbers compared to a smooth bed flow. Chanson [5] showed that the sidewall friction modified the shockwave formation process, and

(A)

(B)

Fig. 7. Photographs of tidal bores in France. (A) Approaching tidal bore of the Sélune river on 7 April 2004, (B) tidal bore of the Dordogne river in Sept. 2006 (Courtesy of Antony Colas) – bore propagation from left to right.

affected significantly the velocity distributions beneath the wave trough.

It is worthwhile noting the usage of modern velocity measurement techniques in recent studies of undular jumps (Table 1). The LDV, PIV, and ADV systems record only the velocity field. But, in undular flows, the pressure gradient is not hydrostatic and detailed experiments should record both pressure and velocity fields. The traditional Prandtl–Pitot tube is still the only instrument that can record simultaneously velocity, pressure and total energy, and the bed shear stress after appropriate calibration [5,41].

3. Positive surges and tidal bores

Positive surges are commonly observed in man-made channels and a related occurrence is the tidal bore in estuaries (Fig. 7). The inception and development of a positive surge are commonly predicted using the method of characteristics and Saint-Venant equations [42]. After formation of the surge, the flow properties immediately upstream and downstream of the front must satisfy the continuity and momentum principles [2,34,43,44]. Eqs. (1) and (2) are valid by introducing the surge Froude number definition: $Fr = (V + U)/\sqrt{g \times d}$ where U is the surge front celerity for an observed standing on the channel bank. A fully-developed positive surge is also called a hydraulic jump in translation.

Positive surges were studied by hydraulicians and applied mathematicians for a few centuries. Major contributions included the works of Barré de Saint-Venant [42], Boussinesq [12], and more recently Lemoine [35], Serre [36] and Benjamin and Lighthill [45]. Several researchers discussed the development of a positive surge [46–49]. Classical experimental investigations of undular surges included Darcy and Bazin [10], Favre [26], Zienkiewicz and Sandover [50], Sandover and Holmes [51], Benet and Cunge [27]. Ponsy and Carbonnell [52] and Treske [28] presented a comprehensive description of positive surges in trapezoidal channels of large sizes. Pertinent reviews comprised Benjamin and Lighthill [45], Sander and Hutter [53] and Cunge [54]. Recent numerical studies encompassed Madsen and Svendsen [55] on the stationary jump, and Caputo and Stepanyants [56], Madsen et al. [57] and El et al. [58] on advancing bores.

To date, most experimental studies were limited to visual observations and sometimes free-surface measurements. For example, Fig. 8 shows some undular surge characteristics. Fig. 8A presents some wave amplitude data including a tidal bore data set (Dee river). Fig. 8B compares the wave steepness a_w/L_w between undular surges and jumps. Previous studies rarely encompassed turbulence except in a few limited studies [29,59,60]. In the following paragraph, recent free-surface and turbulent velocity measurements obtained in a large-size laboratory facility [29,30] are re-analysed. The unsteady flow results provide an unique characterisation of the advancing front, of the unsteady turbulent velocity field in the front, and of the associated turbulent mixing processes in positive surges and tidal bores.

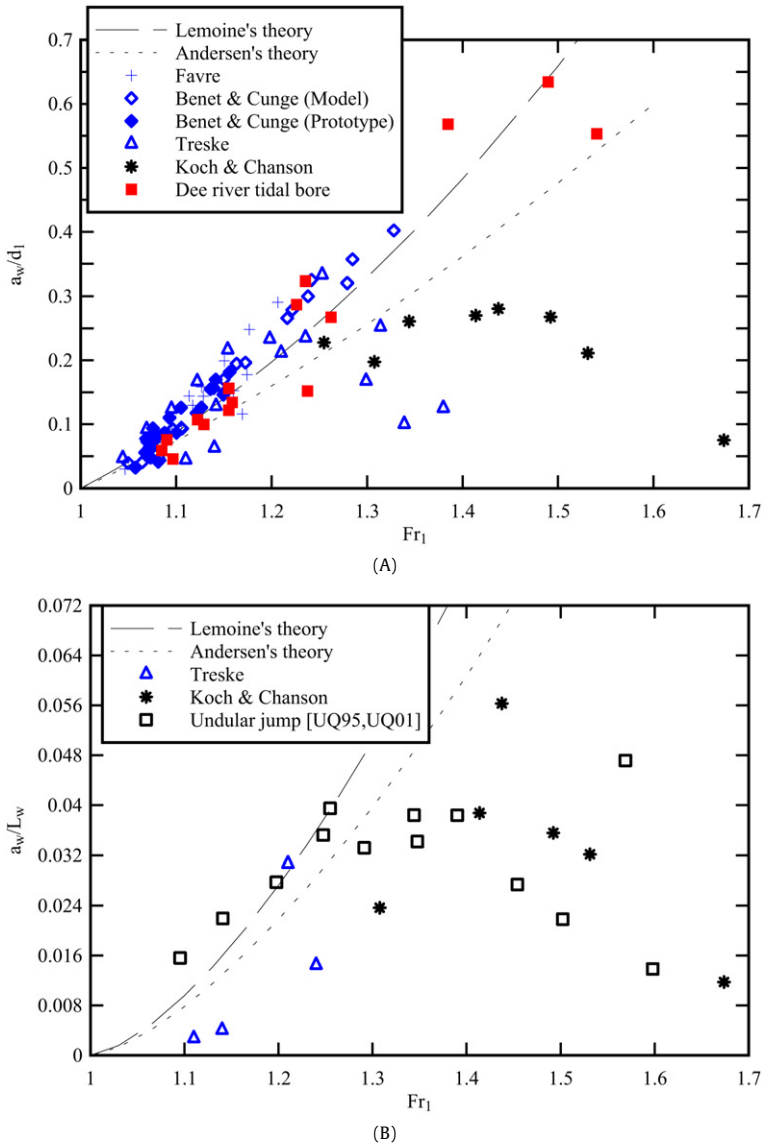

Fig. 8. Undular surge wave. Data: Favre [26], Benet and Cunge [27], Treske [28] Koch and Chanson [29,30], Lewis [31] [Dee river tidal bore]. (A) Dimensionless wave amplitude a_w/d_1. (B) Wave steepness a_w/L_w. Comparison with undular jump data: Chanson [23,7] [UQ95,UQ01].

3.1. Unsteady turbulence beneath surges and bores

Detailed unsteady flow measurements were performed by Koch and Chanson [29] in an undular surge ($Fr_1 = 1.4$) and a positive surge with roller ($Fr_1 = 1.8$) travelling against an initially steady flow. An acoustic Doppler velocimeter (ADV) system was positioned at a fixed location and each experiment was repeated at several vertical elevations y. Figs. 9 and 10 present some typical instantaneous velocity data corresponding to the passage of the surge front above the sampling volume. Each graph presents the dimensionless velocities V_x/V_* and V_z/V_*, and water depth d/d_1, where V_x is the streamwise velocity, V_z is the transverse horizontal velocity, d_1 is the initial water depth and V_* is the shear velocity measured on the channel centreline in the initially steady flow ($V_* = 0.044$ m/s). The time t was zero at 10 seconds prior to the surge front passage at the sampling location, and the surge arrival corresponded to $t \times \sqrt{g/d_1} \approx 90$ (Figs. 9 and 10).

Experimental results indicated systematically some basic flow features. The streamwise velocity component decreased very rapidly with the passage of the bore front. In Figs. 9 and 10, the extent of the horizontal axis corresponds to 9 and 11.7 s respectively. The sudden increase in water depth yielded a slower flow motion to satisfy the conservation of mass. The surge passage was associated with significant fluctuations of the transverse velocity. With the undular surge, the streamwise velocity oscillated with time with the same period as, but out of phase with, the free-surface undulations (Fig. 9). Maximum velocities were observed beneath the wave troughs and minimum velocities below the wave crests. The trend was seen at all vertical and transverse locations, and it was consistent with irrotational flow theory. With the turbulent surge, the velocity records showed some marked difference depending upon the vertical elevation y (Fig. 10). For $y/d_1 > 0.5$, the streamwise velocity component decreased rapidly at the surge front although the streamwise velocity V_x data tended to remain positive beneath the roller toe (Fig. 10B). In contrast, for $y/d_1 < 0.5$, the longitudinal velocity became negative although for a short duration ($104 < t \times \sqrt{g/d_1} < 150$, Fig. 10A). This feature was observed at several transverse locations ($0 < z/B < 0.55$). The existence a sudden streamwise flow reversal indicated some unsteady flow separation, although it was a relatively rapid transient at a fixed point.

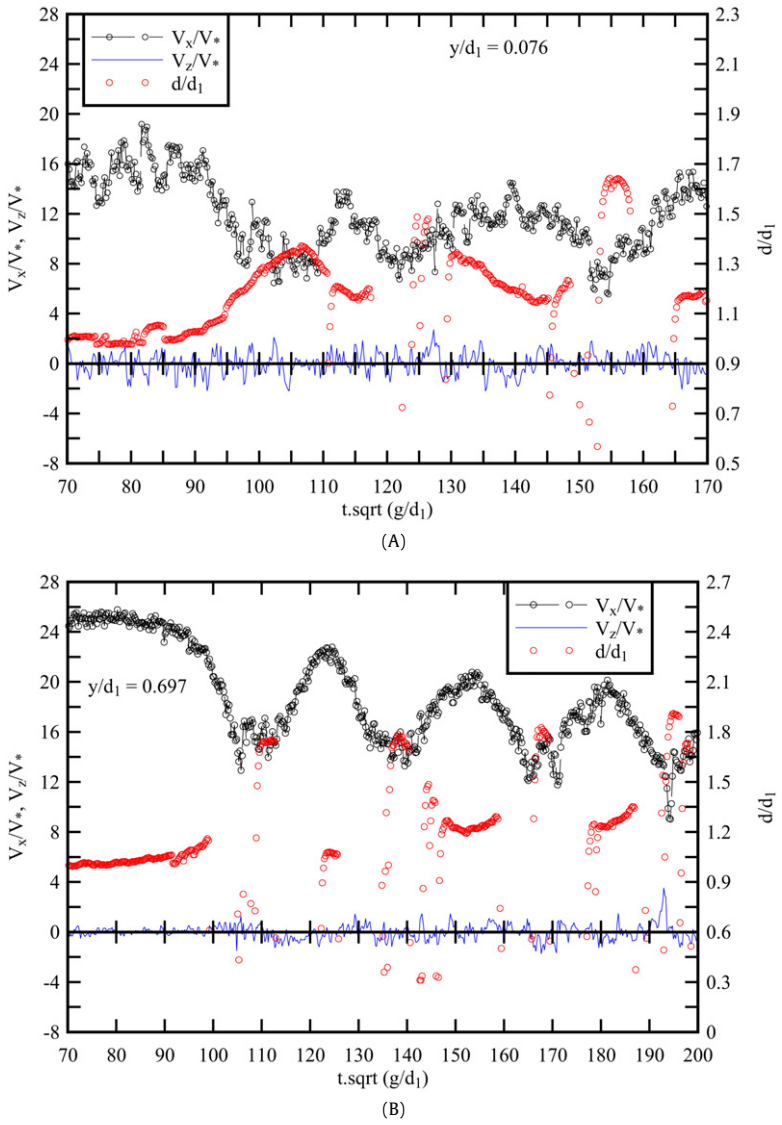

Fig. 9. Instantaneous turbulent velocity measurements V_x/V_* and V_z/V_* beneath an undular positive surge. Data: Koch and Chanson [29,30], $d_1 = 0.080$ m, $Fr_1 = 1.4$, $V_* = 0.044$ m/s. (A) $y/d_1 = 0.076$ (next to the channel bed), (B) $y/d_1 = 0.697$.

The instantaneous Reynolds stresses were calculated using a variable-interval time average VITA technique, where the cutoff frequency was selected such that the averaging time was greater than the characteristic period of fluctuations, and small with respect to the characteristic period for the time-evolution of the mean properties [61]. In undular surge flows, the Eulerian flow properties exhibited an oscillating pattern with a period of about 2.4 s that corresponded to the period of the free-surface undulations. The cut-off frequency was selected as 1 Hz based upon a detailed sensitivity analysis, and the same filtering technique was applied to both streamwise and transverse velocity components, for the undular and breaking surge data. Typical results are shown in Figs. 11 and 12, where the instantaneous shear stress data are plotted together with the measured water depth.

The Reynolds stresses characterised a transport effect resulting from turbulent motion induced by velocity fluctuations with its subsequent increase of momentum exchange and of mixing. The experimental data showed large turbulent stresses, and turbulent stress fluctuations, below the bore front and ensuing flow: i.e., for $t \times \sqrt{g/d_1} > 90$ in Figs. 11 and 12. The Reynolds stress magnitudes were significantly larger than before the surge passage at all vertical elevations. In the undular surge, the largest normal and tangential stresses were observed beneath the wave crests and just before each crest. These turbulent stresses were larger than those beneath the adjacent wave troughs (Fig. 11). Beneath the positive surge with roller, large normal and tangential Reynolds stresses were observed in the upper water column ($y/d_1 > 0.5$) (Fig. 12). It is believed that the sudden increase in normal and tangential turbulent stresses for $0.5 < y/d_1 < 1$ was caused by the passage of the developing mixing layer of the roller. In stationary hydraulic jumps and related flows, researchers observed similarly large Reynolds stresses in and next to the developing shear layer [62–64].

3.2. Turbulent mixing in tidal bores

In macro-tidal estuaries, a tidal bore may form during spring tide conditions when the flood tide is confined to a narrow funnelled channel (Fig. 7). A tidal bore on the Indus river wiped out the fleet of Alexander the Great in B.C. 325 (or B.C. 326 ?) ([65, vol. 2, pp. 156–161, Anabis of Alexander, VI, 19]; [66, p. 233], [1, Book 9]). Both accounts gave a very detailed and accurate description of a tidal bore process. The most famous tidal bores are probably those of the Seine river (France), Qiantang river (China) and

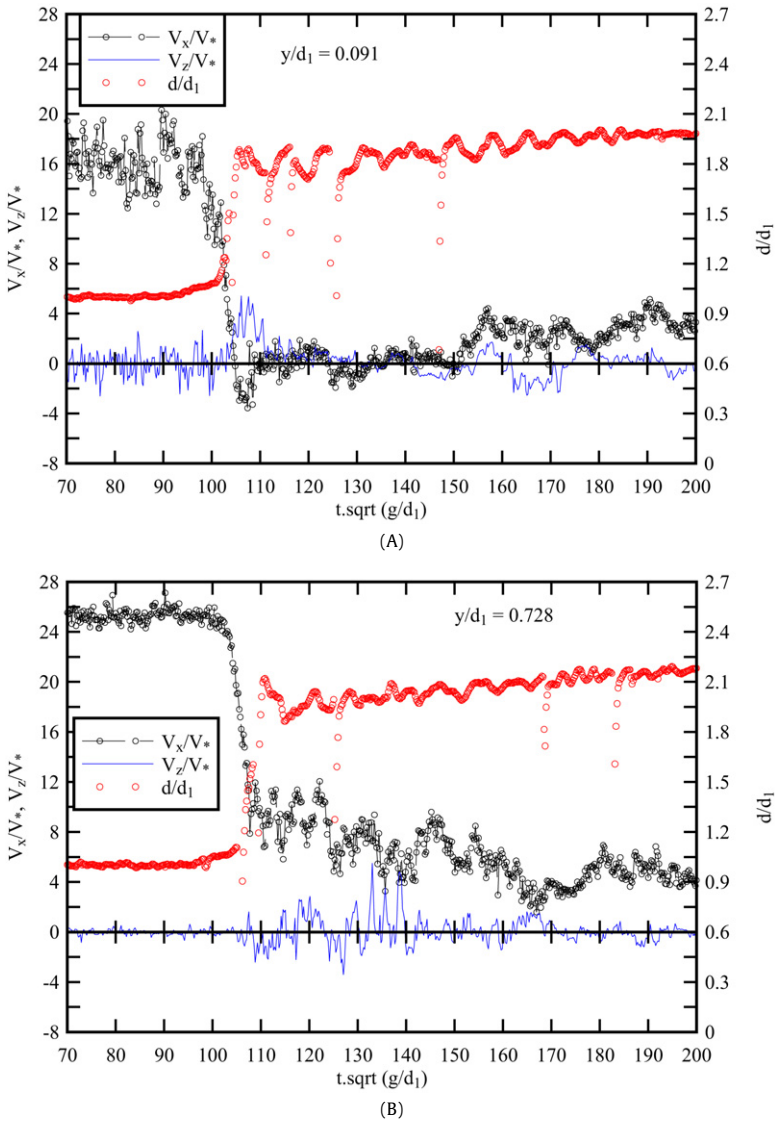

Fig. 10. Instantaneous turbulent velocity measurements V_x/V_* and V_z/V_* beneath a positive surge with roller. Data: Koch and Chanson [29], $d_1 = 0.080$ m, $Fr_1 = 1.8$, $V_* = 0.044$ m/s. (A) $y/d_1 = 0.091$ (next to the channel bed), (B) $y/d_1 = 0.728$.

the "pororoca" of the Amazon river. Smaller tidal bores occur on the Severn and Dee rivers, England, on the Garonne, Dordogne and Sélune rivers, France, at Turnagain Arm and Knik Arm, Cook Inlet (Alaska), in the Bay of Fundy at Petitcodiac and Truro (Canada), on the Styx and Daly rivers (Australia), and at Batang Lupar (Malaysia). Fig. 7 shows photographs of the tidal bores of the Sélune and Dordogne rivers.

The occurrence of tidal bores has a significant impact on river mouths and estuarine systems. Bed erosion and scour take place beneath the bore front while suspended matters are carried upwards in the ensuing wave motion. The process contributes to significant sediment transport with deposition in upstream intertidal areas. Basically tidal bores induce strong mixing and dispersion in the river mouth. Classical mixing theories do not account for such type of discontinuities. Field observations demonstrated strong turbulence and mighty mixing in tidal bores (Fig. 13). Evidences encompassed repeated impact and damage to field measurement equipments: e.g., in Rio Mearim [67]. in the Daly river [68], in the Dee river [69]. Further demonstrations included major damage to river banks and navigation. For example, Captain Moore lost almost his survey ship and two steam cutters when he inadvertently anchored in the Qiantang river estuary in 1888 [70,71]; the Qiantang river banks were repeatedly damaged and overtopped by the tidal bore for centuries (e.g. [72]) (Fig. 13). Other tragic evidences included numerous drownings in tidal bores and "whelps", for example in the Fly river (Papua New Guinea) [73] and Seine river [74].

It was acknowledged that tidal bores induce strong turbulent mixing in estuaries and river mouths: "*in shallow areas, the water boiled violently after the passage of the bore*" [67]. The effects of a tidal bore may be felt along considerable distances when the bore travels far upstream. For example, the Hoogly tidal bore may propagate more than 80 km flowing past the port of Calcutta; the smaller tidal bore of the Sée-Sélune rivers lasts for a few hours and affects more than 15 km of estuarine channels (Fig. 7A). Unusual mixing patterns were reported. Kjerfve and Ferreira [67] presented quantitative measurements of salinity and temperature changes behind the tidal bore of Rio Mearim (Bra.). They recorded sharp jumps in salinity and water temperature about 18 to 42 minutes after the bore passage depending upon the sampling site location. The longest time lag was observed at the most upstream sampling site. During one event on 30 Jan. 1991, a 150 kg sawhorse was toppled down, tumbled for 1.4 km and buried deep into sand. In the Daly river, Wolanski et al. [68] studied the bore passage at a site

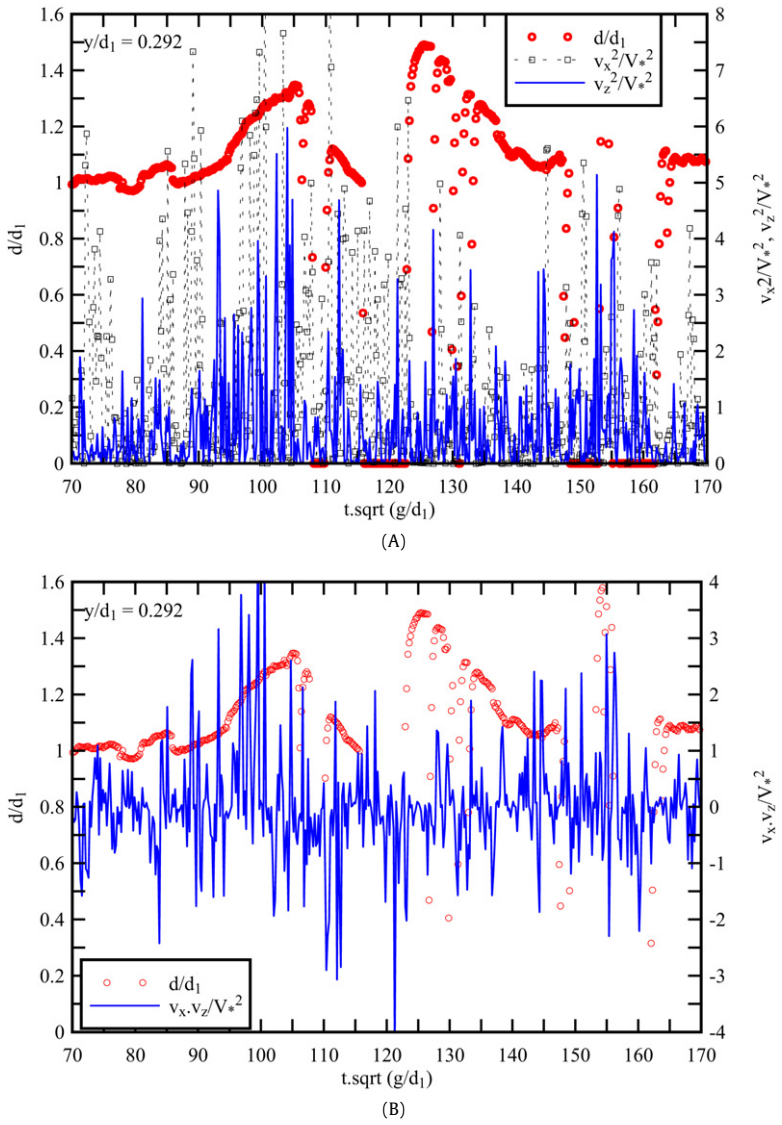

Fig. 11. Turbulent Reynolds stress measurements beneath an undular positive surge. Data: Koch and Chanson [29,30], $d_1 = 0.080$ m, $Fr_1 = 1.4$, $V_* = 0.044$ m/s. (A) Normal stresses v_x^2/V_*^2 and v_z^2/V_*^2 at $y/d_1 = 0.292$, (B) tangential stress $(v_x \times v_z)/V_*^2$ at $y/d_1 = 0.292$.

located 30 to 40 km upstream of the river mouth. On 2 July 2003, a period of strong turbulence was observed for about 3 minutes at about 20 minutes after the bore passage. During this "*turbulence patch*", a tripod holding instruments was toppled down. In the river Mersey (UK), quantitative measurements of salinity behind the bore indicated with a sharp jump about 10–15 minutes after the bore on 12 July 1987 [75]. Unusual flow reversal patterns were seen behind bore fronts in the Seine river and Rio Mearim [67,76]: "*at times, the downstream flow resumed after passage of the bore for another 30 s before the flow again surged upstream*" [67]. The comment was based upon measurements at 0.7 m above the bottom.

3.3. Discussion

The existence of tidal bores is based upon a fragile hydrodynamic balance, which may be easily disturbed by changes in boundary conditions and freshwater inflow. Man-made interventions led to the disappearance of several bores with adverse impacts onto the eco-system: e.g., the mascaret of the Seine river (France) no longer exists and the Colorado river bore (Mexico) is drastically smaller after dredging. Although the fluvial traffic gained in safety in each case, the ecology of estuarine zones were adversely affected. The tidal bores of the Couesnon (France) and Petitcodiac (Canada) rivers almost disappeared after construction of an upstream barrage. At Petitcodiac, this yielded the elimination of several diadromous fish species, including the American shad, Atlantic salmon, Atlantic tomcod, striped bass and sturgeon [77].

There are numerous visual accounts of tidal bores, but field measurements are very limited. Most studies recorded a limited number of parameters with relatively coarse resolutions in terms of time scales, spatial resolutions and velocity magnitudes at a fixed-point. However a tidal bore is a very dynamic process which extends over several kilometres, sometimes tens of kilometres.

The latest turbulence data demonstrated some unique features of tidal bore fronts. Velocity measurements with high-temporal resolution (50 Hz) showed a marked effect of the bore passage (Figs. 9–12). Longitudinal velocities were characterised by rapid flow deceleration at all vertical elevations, while large fluctuations of transverse velocities were recorded beneath the front (Figs. 9 and 10). Instantaneous Reynolds stress data highlighted large turbulent stress magnitudes and turbulent stress fluctuations during the passage and behind the bore front at all vertical elevations (Figs. 11 and 12). Hence bed erosion may take place during the

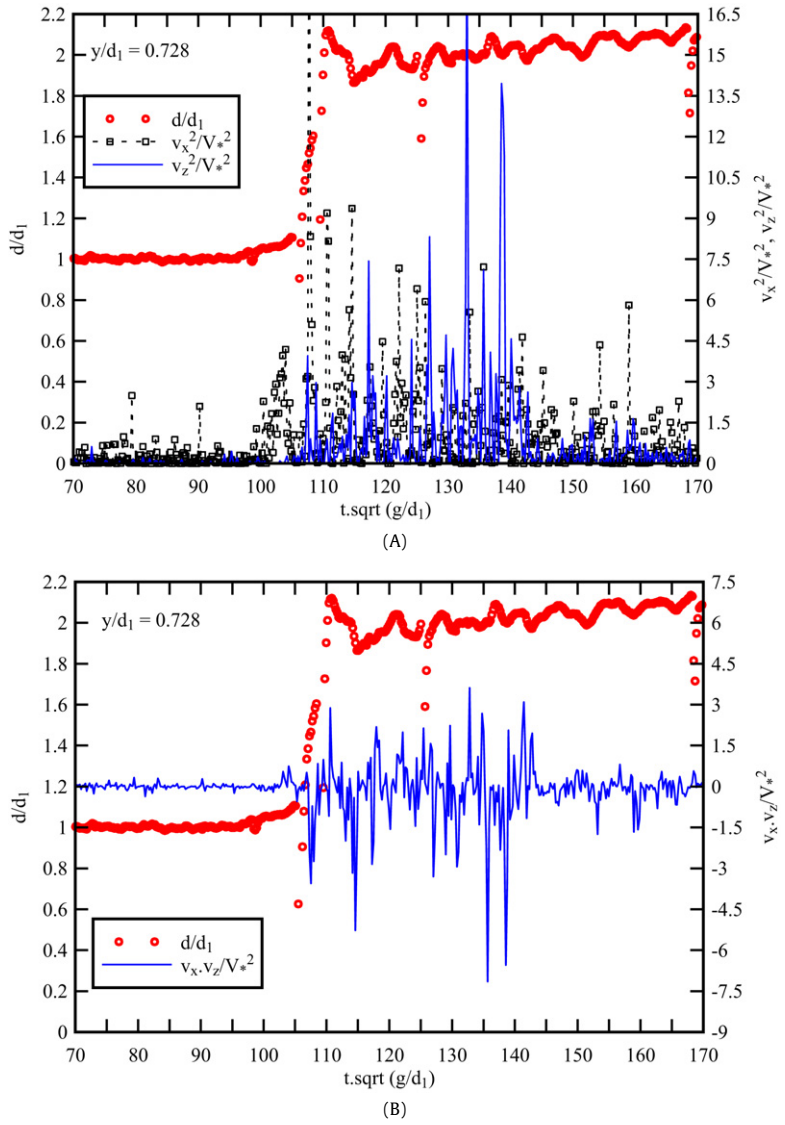

Fig. 12. Turbulent Reynolds stress measurements beneath a positive surge with roller, Data: Koch and Chanson [29], $d_1 = 0.080$ m, $Fr_1 = 1.8$, $V_* = 0.044$ m/s. (A) Normal stresses v_x^2/V_*^2 and v_z^2/V_*^2 at $y/d_1 = 0.728$, (B) tangential stress $(v_x \times v_z)/V_*^2$ at $y/d_1 = 0.728$.

Fig. 13. Turbulence in the Qiantang river of tidal bore on 11 Nov. 2003 (Courtesy of Dr C. Liu) – view from the left bank with bore propagation from left to right.

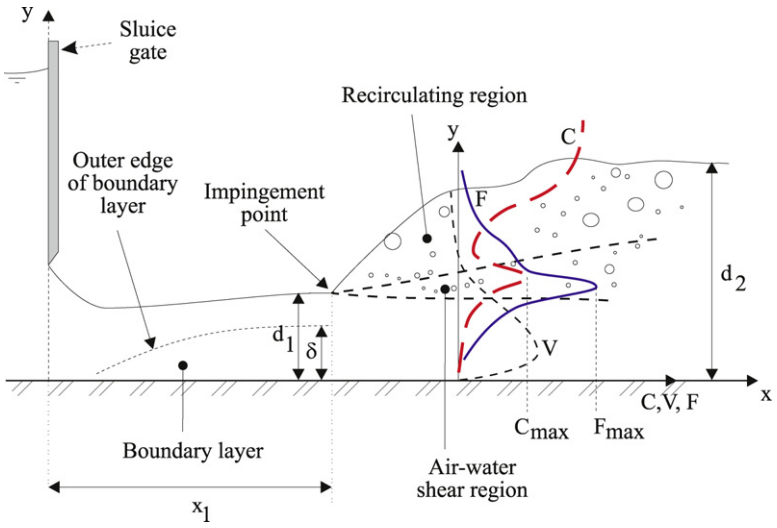

Fig. 14. Air bubble entrainment in hydraulic jumps: definition sketch.

surge front passage, and the eroded material and other scalars are advected in the "whelps" and wave motion behind the tidal bore front. These would be consistent with very-strong turbulent mixing observed in tidal bore affected estuaries, associated with accretion and deposition in the upper estuarine zones. Simply tidal bores do have a significant impact on an estuarine system.

4. Air bubble entrainment in hydraulic jumps: dynamic similarity and scale effects

A characteristic feature of turbulent hydraulic jumps with roller is the large amount of entrained air bubbles (Fig. 1B). Air bubbles and air packets are entrapped at the impingement of the high-velocity inflow into the roller. The entrained bubbles are advected in a developing shear layer (Fig. 14). The jump toe ($x = x_1$, $y = d_1$) represents a flow singularity which is a source of both air bubbles and vorticity. The developing shear region is the locus of a double diffusion process whereby vorticity and air bubbles diffuse at a different rate and in a different manner downstream of the impingement point [78,79].

The initial investigations of air bubble entrainment in hydraulic jumps focused on the total quantity of entrained air in closed-conduits (e.g. [80,81]). The first successful two-phase flow measurements in hydraulic jumps were performed by Rajaratnam [82]. A milestone contribution was the work of Resch and Leutheusser [83] who showed that the bubble entrainment process, momentum transfer and energy dissipation are strongly affected by the inflow conditions. Chanson [84] studied particularly the air–water properties in partially-developed hydraulic jumps, showing some similarity with air entrainment in plunging jets. Mossa and Tolve [85] recorded instantaneous properties of bubbly flow structures using an imaging technique. Chanson and Brattberg [79] documented the vertical distributions of void fractions, bubble count rates and air–water velocities in the shear layer and roller region of hydraulic jumps with relatively large inflow Froude numbers. Murzyn et al. [86] measured detailed air–water flow properties in hydraulic jumps with low inflow Froude numbers. Chanson [87] characterised the turbulent eddies and the bubbly flow microstructures. However little information is available on the dynamic similarity relevant to air–water flow properties and on the scale effects affecting the air entrapment and advection processes [88].

4.1. Dimensional analysis and dynamic similarity

For a hydraulic jump in a horizontal, rectangular channel, a simplified dimensional analysis shows that the parameters affecting the two-phase flow properties at a position (x, y, z) within the jump are: (a) the fluid properties including the air and water densities ρ_{air} and ρ, the air and water dynamic viscosities μ_{air} and μ, the surface tension σ, and the gravity acceleration g, (b) the channel properties including the width B, and, (c) the inflow properties such as the inflow depth d_1, the inflow velocity V_1, a characteristic turbulent velocity u'_1, and the boundary layer thickness δ. The air–water flow properties may be expressed as:

$$C, F, V, u', d_{ab} \ldots = F_1(x, y, z, d_1, V_1, u'_1, x_1, \delta, B, g, \rho_{air}, \rho_w, \mu_{air}, \mu_w, \sigma, \ldots) \quad (5)$$

where C is the void fraction, F is the bubble count rate, V is the velocity, u' is a characteristic turbulent velocity, d_{ab} is a bubble size, x is the coordinate in the flow direction measured from the nozzle, y is the vertical coordinate, z is the transverse coordinate measured from the channel centreline, and x_1 is the distance from the upstream gate (Fig. 14). In addition, biochemical properties of the water solution may be considered. If the local void fraction C is known, the density and viscosity of the air–water mixture may be expressed in terms of the water properties and void fraction only; hence the parameters ρ_{air} and μ_{air} may be ignored.

Since the relevant length scale is the upstream flow depth d_1, Eq. (3) may be transformed in dimensionless terms:

$$C, \frac{F \times d_1}{V_1}, \frac{V}{\sqrt{g \times d_1}}, \frac{u'}{V_1}, \frac{d_{ab}}{d_1} \ldots = F_2\left(\frac{x}{d_1}, \frac{y}{d_1}, \frac{z}{d_1}, \frac{V_1}{\sqrt{g \times d_1}}, \frac{u'_1}{V_1}, \rho \times \frac{V_1 \times d_1}{\mu}, \rho \times \frac{V_1^2 \times d_1}{\sigma}, \frac{x_1}{d_1}, \frac{\delta}{d_1}, \frac{B}{d_1}\right) \quad (6)$$

In Eq. (6), the dimensionless air–water flow properties (left hand-side terms) at a dimensionless position $(x/d_1, y/d_1, z/d_1)$ are expressed as functions of the dimensionless inflow properties and channel geometry. In the right-hand side of Eq. (6), the fourth, sixth and seventh terms are the inflow Froude, Reynolds and Weber numbers respectively. Any combination of these numbers is also dimensionless and may be used to replace one of the combi-

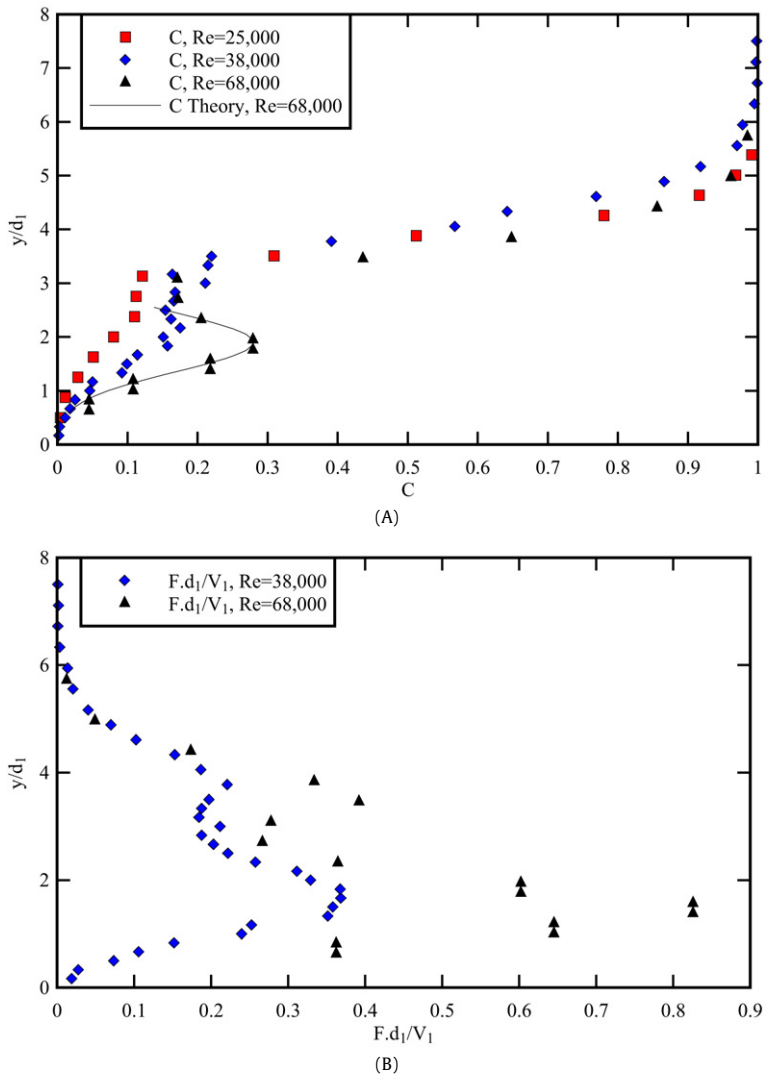

Fig. 15. Effects of the inflow Reynolds number on the dimensionless distributions of void fraction C and bubble count rate $F \times d_1/V_1$ for $Fr_1 = 5.1$, $x_1/d_1 = 42$, $B/d_1 \geqslant 20$ and $(x - x_1)/d_1 = 8$, $Re = 25{,}000$, 38,000 and 68,000. Data: Chanson [88], Murzyn and Chanson [91] (A) Dimensionless distributions of void fraction – comparison with Eq. (9), (B) dimensionless distributions of bubble count rate.

nations. In particular one parameter can be replaced by the Morton number $Mo = g \times \mu^4/(\rho \times \sigma^3)$ since:

$$Mo = \frac{We^3}{Fr^2 \times Re^4} \tag{7}$$

The Morton number is a function only of fluid properties and gravity constant, and it becomes an invariant if the same fluids (air and water) are used in both model and prototype.

Chanson [88] tested the effects of the relative channel width B/d_1, with all other dimensionless parameters being constant, for $Fr_1 = 5$ and 8.5, and $Re = 70{,}000$ to 95,000 where Fr_1 and Re are respectively the inflow Froude and Reynolds numbers. The results showed that the relative channel width had no effect on the two-phase flow properties for $B/d_1 \geqslant 10$. Within these conditions, Eq. (6) becomes:

$$C, \frac{F \times d_1}{V_1}, \frac{V}{\sqrt{g \times d_1}}, \frac{u'}{V_1}, \frac{d_{ab}}{d_1} \ldots = F_3\left(\frac{x}{d_1}, \frac{y}{d_1}, \frac{z}{d_1}, Fr_1, \frac{u'_1}{V_1}, Re, Mo, \frac{x_1}{d_1}, \frac{\delta}{d_1}\right) \tag{8}$$

In the study of hydraulic jumps, theoretical considerations showed the significance of the inflow Froude number [1] and a Froude similitude is commonly used (e.g. [2,44,89]). However the entrapment of air bubbles and the mechanisms of air bubble breakup and coalescence are dominated by surface tension effects, while turbulent processes in the shear region are dominated by viscous forces [78,90]. Dynamic similarity of air bubble entrainment in hydraulic jumps becomes impossible because of too many relevant parameters (Froude, Reynolds and Morton numbers) in Eq. (8).

Table 3
Physical modelling of two-phase flow properties in hydraulic jumps based upon an undistorted Froude similitude with air and water

Ref.	x_1 (m)	d_1 (m)	Fr_1	Re	B (m)
Chanson [88]	1.0	0.024	5.1	68,000	0.50
			8.6	98,000	
Murzyn and Chanson [91,92]	0.75	0.018	5.1	38,000	0.50
			8.3	62,000	
Chanson [88]	0.5	0.012	5.1	25,000	0.25
			8.4	38,000	

Recently some experiments were conducted with the same inflow Froude numbers to test the validity of the Froude similarity in terms of the two-phase flow properties in hydraulic jumps with reference to the effects of the Reynolds number [88,91]. Three series of experiments were designed to be geometrically similar based upon a Froude similitude with undistorted scale (Table 3).

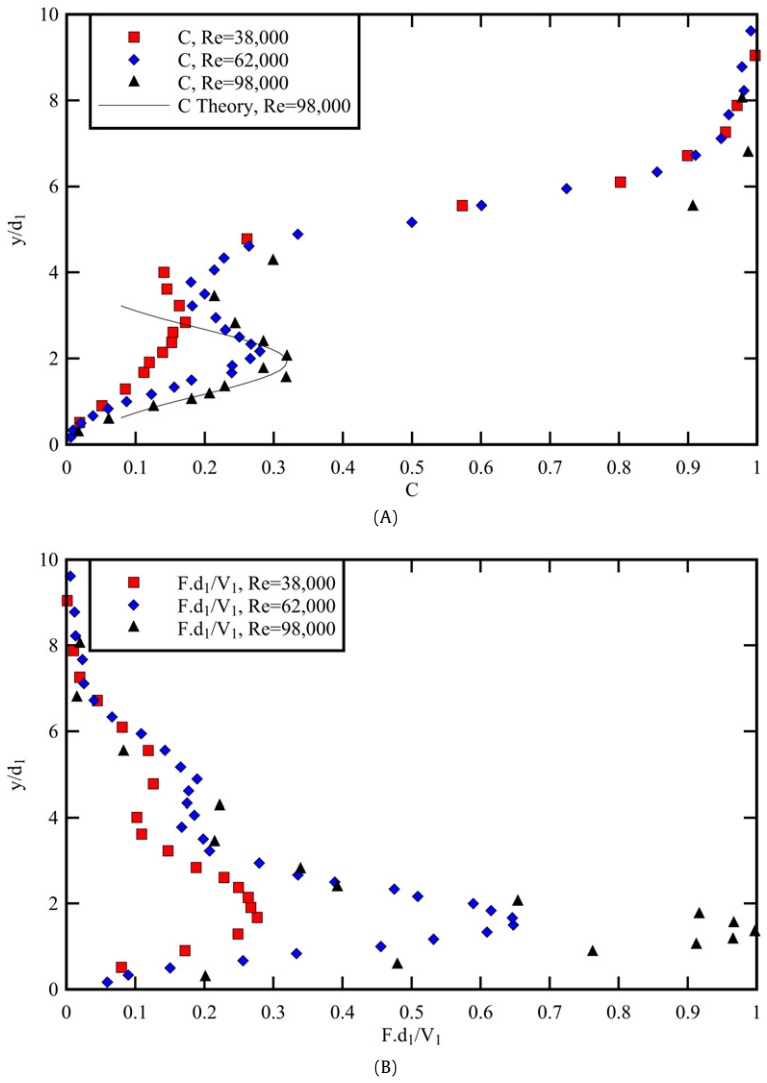

Fig. 16. Effects of the inflow Reynolds number on the dimensionless distributions of void fraction C and bubble count rate $F \times d_1/V_1$ for $Fr_1 = 8.5$, $x_1/d_1 = 42$, $B/d_1 \geqslant 20$ and $(x - x_1)/d_1 = 12$, $Re = 38{,}000$, 62,000 and 98,000. Data: Chanson [88], Murzyn and Chanson [91]. (A) Dimensionless distributions of void fraction – comparison with Eq. (9), (B) dimensionless distributions of bubble count rate.

The geometric scaling ratio was $L_{scale} = 2.0$ between the smallest and largest series of experiments, where L_{scale} is the geometric scaling ratio defined as the ratio of prototype to model dimensions, and $L_{scale} = 1.33$ between the largest series of experiments and the intermediate one. Similar experiments were conducted for identical Froude numbers $Fr = 5.1$ and 8.5 with identical upstream distance between gate and jump toe x_1/d_1. For an identical Froude number, the air–water flow measurements were performed in the developing air–water flow region at identical cross-sections $(x - x_1)/d_1 < 20$.

4.2. Two-phase flow properties in turbulent hydraulic jumps

A turbulent hydraulic jump is characterised by the development of large-scale turbulence, surface waves and spray, energy dissipation and air entrainment (Fig. 1B). Air bubbles and air packets are entrained at the jump toe into a free shear layer characterised by intensive turbulence production, predominantly in vortices with horizontal axes perpendicular to the flow direction (Fig. 14). Air can be entrained by a combination of different mechanisms. If the inflow is aerated upstream of the intersection with the pool of water, the aerated layer at the jet free-surface is entrained past the impingement point. This process is also called pre-entrainment or two-phase flow air flux. Further an air layer is set into motion by shear friction next to the free-surface of the impinging flow and some air is trapped at the entrainment point. Another mechanism is the aspiration of the induction trumpet formed at the intersection of the water jet with the roller (i.e. jump toe). At the closure of the trumpet, air packets are entrapped and entrained within the shear flow (e.g. [93]).

In a hydraulic jump with partially-developed inflow, the void fraction distributions exhibited a characteristic peak C_{max} in the turbulent shear layer [79,84,86]. This feature is sketched in Fig. 14 and experimental data are shown in Figs. 15A and 16A. The maximum void fraction C_{max} in the shear layer decreased with increasing distance $(x - x_1)/d_1$ from jump toe, while the diffusion layer broadened. The interactions between developing shear layer and air diffusion layer were complicated, and they were believed to be responsible for the existence of a peak F_{max} in bubble count rate seen in Figs. 15B and 16B. Figs. 15B and 16B present dimensionless distributions of bubble count rate. The bubble count rate F is defined as the number of bubbles detected by the probe sensor per unit time, and it is proportional to the air–water interfacial area.

Experimental observations showed that the location where the bubble count rate is maximum ($F = F_{max}$) did not coincide with the locus of maximum void fraction $C = C_{max}$ (Figs. 15 and 16).

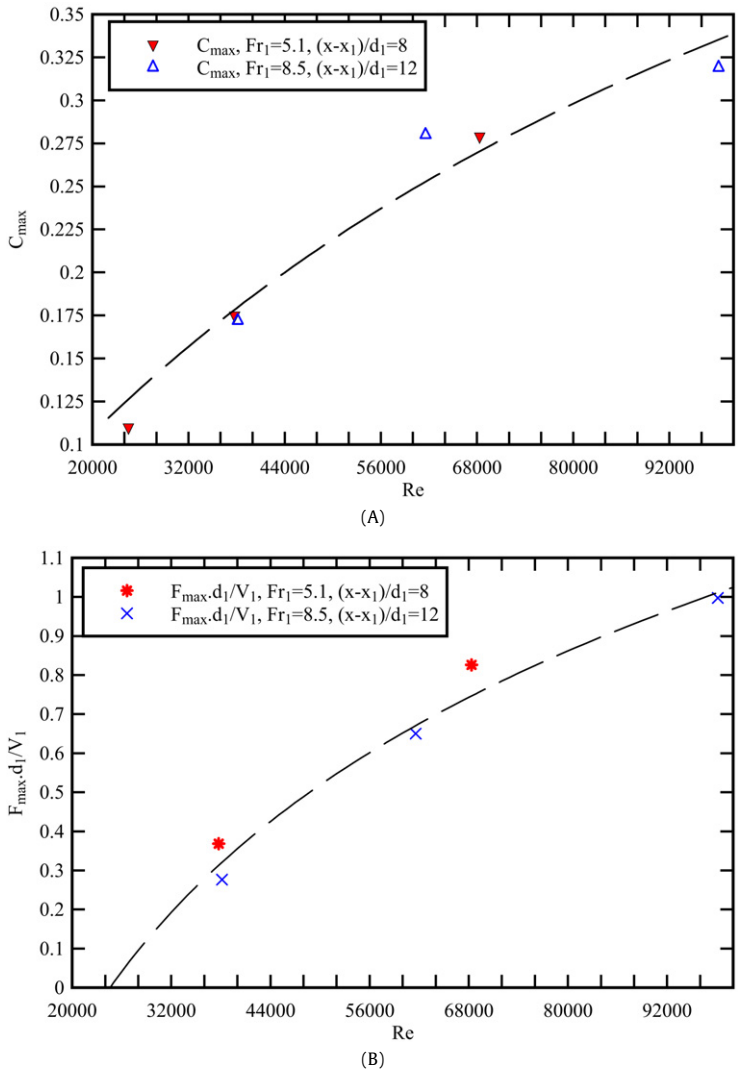

Fig. 17. Effects of the inflow Reynolds number on the maximum void fraction C_{max} and maximum dimensionless bubble count rate $F_{max} \times d_1/V_1$ in the shear layer for a given inflow Froude number Fr_1. Data: Chanson [88], Murzyn and Chanson [91]. (A) Effects of inflow Reynolds number on the maximum void fraction in the shear layer, (B) effects of inflow Reynolds number on the maximum dimensionless bubble count rate in the shear layer.

In the air diffusion layer, the analytical solution of the advective diffusion equation for air bubbles yields the void fraction profile [78,94]:

$$C = \frac{Q_{air}/Q}{\sqrt{4\pi D^{\#}(x-x_1)/d_1}}\left(\exp\left(-\frac{(y/d_1-1)^2}{4D^{\#}(x-x_1)/d_1}\right) + \exp\left(-\frac{(y/d_1+1)^2}{4D^{\#}(x-x_1)/d_1}\right)\right) \quad (9)$$

where Q_{air} is the volume flow rate of entrained air, Q is the water discharge, $D_{\#}$ is a dimensionless diffusivity: $D_{\#} = D_t/(V_1 \times d_1)$, and D_t is the air bubble turbulent diffusivity. Eq. (9) is valid for both two-dimensional supported plunging jet and hydraulic jump flows. It is compared with experimental data in Figs. 15A and 16A.

A comparative analysis of the data sets (Table 3) showed drastic scale effects in the smaller hydraulic jumps in terms of void fraction, bubble count rate and bubble chord time distributions. The results highlighted consistently a more rapid de-aeration of the jump roller with decreasing Reynolds number for a given inflow Froude number, an absence of self-similarity of the void fraction profiles in the developing shear layer for $Re < 40{,}000$ for $Fr_1 = 5.1$ (Fig. 15A), and an increasing dimensionless bubble count rate with increasing Reynolds number for a given inflow Froude number (Fig. 15B and 16B). The bubble chord time distributions were more skewed with increasing Reynolds number for a given inflow Froude number, and the bubble chord times were not scaled according to a Froude similitude.

For a given inflow Froude number, the effects of the Reynolds number on the two-phase flow properties were particularly marked in the developing shear layer. This is illustrated in Fig. 17 showing the maximum void fraction C_{max} and maximum dimensionless bubble count rate $F_{max} \times d_1/V_1$ in the shear layer for a given inflow Froude number Fr_1 as functions of the inflow Reynolds number Re. The data are compared with best fit trends (dashed lines, Fig. 17). The results indicated some monotonic increase in maximum void fraction and maximum dimensionless bubble count rate in the mixing layer with increasing Reynolds number (Fig. 17). The rates of increase were about the same for both inflow Froude numbers $Fr_1 = 5.1$ and 8.5 and they did not show any asymptotic trend. Basically the data collected with $Re = 2 \times 10^4$ could not be extrapolated to $Re = 10^5$ without significant scale effects. Further the lack of asymptotic trend, implied that the present data sets with Reynolds numbers up to 10^5 cannot be extrapolated to large-size prototype structures without significant scale effects in terms of void fraction, bubble count rate and bubble chord time distributions. This result has important implications in civil, environmental and sanitary engineering design. In hydraulic structures,

Fig. 18. Hydraulic jump at the spillway toe of Chinchilla minimum energy loss weir on 8 Nov. 1997.

storm water systems and water treatment facilities, hydraulics jumps may be experienced with Reynolds numbers ranging from 10^6 to over 10^8. Fig. 18 illustrates a prototype spillway flow situation with hydraulic jump Reynolds number of about 10^7. The supercritical flow down the concrete spillway chute (Fig. 18, left) impacts the deep tailwaters resulting in a hydraulic jump. Note the brown colour of the waters because of the presence of suspended sediments, yielding a three-phase (water–air-sediment) flow in the hydraulic jump roller.

In a physical model, the flow conditions are said to be similar to those in the prototype if the model displays similarity of form (geometric similarity), similarity of motion (kinematic similarity) and similarity of forces (dynamic similarity) [89]. Scale effects may exist when one or more relevant dimensionless parameters have different values in the model and prototype. Eq. (6) highlighted that the study of air bubble entrainment in hydraulic jumps required a large number of relevant parameters [88]. The present analysis demonstrated further that dynamic similarity of two-phase flows in hydraulic jumps cannot be achieved with a Froude similitude unless working at full-scale (1:1). In experimental facilities with Reynolds numbers up to 10^5, some viscous scale effects were observed in terms of the rate of entrained air (void fraction), air–water interfacial area (bubble count rate) and bubble size populations (bubble chord time distributions) (Figs. 15–17).

5. Conclusion

In an open channel, a hydraulic jump is a relatively short and turbulent flow. Its one-dimensional flow properties may be solved using the continuity and momentum principles [1]. But, the present knowledge of the turbulent flow field is fairly limited especially in environmental and geophysical flow processes such as those illustrated in Figs. 1, 7, 13 and 18.

The complicated nature of the undular hydraulic jump is described and illustrated by experimental means. The undular flow is subjected to rapid pressure and velocity redistributions between adjacent troughs and crests. The interactions between boundary friction and free-surface flow play a major role and they are responsible for basic differences between undular surges and jumps. The positive surge is an unsteady form of hydraulic jump which may be solved using the continuity and momentum principles. A challenging environmental application is the tidal bore, and the understanding of turbulence beneath a propagating surge is essential to comprehend the basic sediment transport processes. The turbulent hydraulic jump with roller is characterised by strong air bubble entrainment, spray and splashing. Basic dimensional consideration, supported by experimental evidences, showed that Froude-similar experiments are affected by some drastic scale effects in terms of void fraction, bubble count rate and bubble chord time distributions. Experimental results obtained with Reynolds numbers up to 10^5 cannot be extrapolated to large-size prototype flows without significant scale effects.

After centuries of research, the hydraulic jump remains a fascinating flow motion and the present knowledge is insufficient in several areas: e.g., gas entrainment, turbulence, undular flow. The present expertise lacks further experimental observations at the geophysical scales: i.e., with Reynolds number of 10^6 and above. Numerical modelling of hydraulic jumps may be a future research direction. The numerical approach is not simple because the hydraulic jump flow encompasses many challenges including interactions between vortical structures and free-surface, and two-phase flow turbulence. Some numerical techniques (LES, VOF) can be applied to turbulent flows with large Reynolds numbers, but they lack microscopic resolutions and are not always applicable to two-phase flows. Other numerical techniques (DNS) provide a greater level of small-scale details but are limited to turbulent flows with relatively small Reynolds numbers. Future studies of hydraulic jumps may be based upon some composite models linking up numerical and physical studies.

Glossary

Bélanger equation: momentum equation applied across a hydraulic jump in a horizontal channel; the equation was named after Jean-Baptiste Bélanger.
Éteules: French for whelps.
Fawer jump: undular hydraulic jump.
Hydraulic jump: stationary transition from a rapid, high-velocity flow to a slower fluvial flow motion.
Mascaret: French for tidal bore.
Pororoca: tidal bore of the Amazon river in Brazil.
Positive surge: a positive surge results from a sudden increase in flow depth. It is an abrupt wave front. The unsteady flow conditions may be solved as a quasi-steady flow situation and a positive surge is called a hydraulic jump in translation.
Rapidly varied flow: is characterised by large changes over a short distance (e.g. sharp-crested weir, sluice gate, hydraulic jump).
Roller: in hydraulics, a series of large-scale turbulent eddies: e.g., the roller of a hydraulic jump.

Shock waves: in a high-velocity, supercritical flows, a flow disturbance (e.g. change of direction, contraction) induces the development of shock waves propagating at the free-surface across the channel. Shock waves are called also lateral shock waves, oblique hydraulic jumps, Mach waves, cross-waves, diagonal jumps.

Stilling basin: hydraulic structure for dissipating the energy of the flow downstream of a spillway, outlet work, chute or canal structure. In many cases, a hydraulic jump is used as the energy dissipator within the stilling basin.

Surge: a surge in an open channel is a sudden change of flow depth (i.e. abrupt increase or decrease in depth). An abrupt increase in flow depth is called a positive surge while a sudden decrease in depth is termed a negative surge.

Supercritical flow: flow characterised by a Froude number greater than unity.

Tidal bore: positive surge of tidal origin, developing in an estuary as the tide turns to rising.

Undular hydraulic jump: stationary hydraulic jump characterised by steady stationary free-surface undulations downstream of the jump and by the absence of a formed roller. An undular jump flows is called Fawer jump in homage to Fawer's work.

Undular surge: positive surge characterised by a train of secondary waves (or undulations) following the surge front. Undular surges are sometimes called Boussinesq–Favre waves in homage to the contributions of Josepth Boussinesq and H. Favre.

Weak jump: a weak hydraulic jump is characterised by a marked roller, no free-surface undulation and low energy loss. It is usually observed after the disappearance of undular hydraulic jump with increasing upstream Froude numbers.

Whelps: waves behind the leading edge of the tidal bore front. For an observer standing on the bank, the whelps are the wave trains seen after the surge front passage.

Acknowledgements

Hubert Chanson acknowledges the contributions of his colleagues, co-workers and research students, in particular Dr Sergio Montes, Christian Koch, Dr Frédéric Murzyn, and the technical assistance of Graham Illidge and Clive Booth.

References

[1] J.B. Bélanger, Essai sur la Solution Numérique de quelques Problèmes Relatifs au Mouvement Permanent des Eaux Courantes, Carilian-Goeury, Paris, France, 1828 (in French).
[2] F.M. Henderson, Open Channel Flow, MacMillan Company, New York, USA, 1966.
[3] H. Chanson, J.S. Montes, Characteristics of undular hydraulic jumps. Experimental apparatus and flow patterns, J. Hyd. Engrg., ASCE 121 (2) (1995) 129–144. Discussion: 123 (2) 161–164.
[4] J.S. Montes, H. Chanson, Characteristics of undular hydraulic jumps. Results and calculations, J. Hyd. Engrg., ASCE 124 (2) (1998) 192–205.
[5] H. Chanson, Boundary shear stress measurements in undular flows: Application to standing wave bed forms, Water Res. Res. 36 (10) (2000) 3063–3076.
[6] I. Ohtsu, Y. Yasuda, H. Gotoh, Hydraulic condition for undular-jump formations, J. Hyd. Res., IAHR 39 (2) (2001) 203–209. Discussion: 2002 40 (3), 379–384.
[7] H. Chanson, Physical modelling of the flow field in an undular tidal bore, J. Hyd. Res., IAHR 43 (3) (2005) 234–244.
[8] J.M. Lennon, D.F. Hill, Particle image velocimetry measurements of undular and hydraulic jumps, J. Hyd. Engrg. 132 (12) (2006) 1283–1294.
[9] M. Ben Meftah, F. De Serio, M. Mossa, A. Pollio, Analysis of the velocity field in a large rectangular channel with lateral shockwave, Env. Fluid Mech. 7 (6) (2007) 519–536. doi:10.1007/s10652-007-9034-7.
[10] H.P.G. Darcy, H.E. Bazin, Recherches hydrauliques, Imprimerie Impériales, Paris, France, Parties 1ère et 2ème, 1865 (in French).
[11] G. Bidone, Le Remou et sur la Propagation des Ondes, Report to Académie Royale des Sciences de Turin, séance 12 Dec., vol. XXV, 1819, pp. 21–112 & 4 plates (in French).
[12] J.V. Boussinesq, Essai sur la Théorie des Eaux Courantes, Mémoires présentés par divers savants à l'Académie des Sciences, Paris, France, vol. 23, Série 3 (1), supplément 24, 1877, pp. 1–680 (in French).
[13] B.A. Bakhmeteff, Hydraulics of Open Channels, first ed., McGraw-Hill, New York, USA, 1932, 329 p.
[14] W.H. Hager, Energy Dissipators and Hydraulic Jump, Water Science and Technology Library, vol. 8, Kluwer Academic Publ., Dordrecht, The Netherlands, 1992, 288 p.
[15] J.M. Aristoff, J.D. Leblanc, A.E. Hosoi, J.W.M. Bush, Viscous hydraulic jumps, Phys. Fluids 16 (9) (2004) S4.
[16] R.H. Clarke, The morning glory: an atmospheric hydraulic jump, J. Appl. Meteorology 11 (1972) 304–311.
[17] R.H. Clarke, R.K. Smith, D.G. Reid, The morning glory of the Gulf of Carpentaria – an atmospheric undular bore, Monthly Weather Rev. 109 (8) (1981) 1726–1750.
[18] B.A. Bakhmeteff, A.E. Matzke, The Hydraulic jump in terms of dynamic similarity, Trans. ASCE 101 (1936) 630–647. Discussion: 101, 648–680.
[19] A.M. Binnie, J.C. Orkney, Experiments on the flow of water from a reservoir through an open channel. II. The formation of hydraulic jump, Proc. Roy. Soc. London Ser. A 230 (1955) 237–245.
[20] C. Fawer, Etude de Quelques Ecoulements Permanents à Filets Courbes, Thesis, Lausanne, Switzerland, Imprimerie La Concorde, 1937, 127 p. (in French).
[21] J.S. Montes, A study of the undular jump profile, in: Proc. 9th Australasian Fluid Mechanics Conference AFMC, Auckland, New Zealand, 1986, pp. 148–151.
[22] A.A. Ryabenko, Conditions favorable to the existence of an undulating jump, Gidrotekhnicheskoe Stroitel'stvo 12 (1990) 29–34 (in Russian). Translated in Hydrotechnical Construction, 1990, Plenum Publ., pp. 762–770.
[23] H. Chanson, Flow characteristics of undular hydraulic jumps. Comparison with near-critical flows, Report CH45/95, Dept. of Civil Engineering, University of Queensland, Australia, 1995, June, 202 p.
[24] F. Engelund, J. Munch-Petersen, Steady flow in contracted and expanded rectangular channels. Some considerations concerning the shape of the water surface J. La Houille Blanche (Aug./Sept. 1953) 464–474.
[25] V.M. Andersen, Undular hydraulic jump, J. Hyd. Div. ASCE 104 (HY8) (1978) 1185–1188. Discussion: 105 (HY9) 1208–1211.
[26] H. Favre, Etude Théorique et Expérimentale des Ondes de Translation dans les Canaux Découverts, Dunod, Paris, France, 1935 (in French).
[27] F. Benet, J.A. Cunge, Analysis of experiments on secondary undulations caused by surge waves in trapezoidal channels, J. Hyd. Res., IAHR 9 (1) (1971) 11–33.
[28] A. Treske, Undular bores (favre-waves) in open channels – experimental studies, J. Hyd. Res., IAHR 32 (3) (1994) 355–370. Discussion: 33 (3), 274-278.
[29] C. Koch, H. Chanson, An experimental study of tidal bores and positive surges: Hydrodynamics and turbulence of the bore front, Report No. CH56/05, Dept. of Civil Engineering, The University of Queensland, Brisbane, Australia, July 2005, 170 p.
[30] C. Koch, H. Chanson, Turbulent mixing beneath an undular bore front, J. Coastal Res. 24 (4) (2008) 999–1007. doi:10.2112/06-0688.1.
[31] A.W. Lewis, Field studies of a tidal bore in the River Dee, M.Sc. thesis, Marine Science Laboratories, University College of North Wales, Bangor, UK, 1972.
[32] A.T. Ippen, R.F. Harleman, Verification of theory for oblique standing waves, Trans. ASCE 121 (1956) 678–694.
[33] H. Rouse, Fluid Mechanics for Hydraulic Engineers, McGraw-Hill Publ., New York, USA, 1938, also Dover Publ., New York, USA, 1961, 422 p.
[34] J.A. Liggett, Fluid Mechanics, McGraw-Hill, New York, USA, 1994.
[35] R. Lemoine, Sur les ondes positives de translation dans les canaux et sur le ressaut ondulé de faible amplitude, J. La Houille Blanche (March–April 1948) 183–185 (in French).
[36] F. Serre, Contribution à l'etude des ecoulements permanents et variables dans les canaux, J. La Houille Blanche (Dec. 1953) 830–872 (in French).
[37] Y. Iwasa, Undular jump and its limiting conditions for existence, in: Proc. 5th Japan National Congress for Applied Mechanics, Japan, Paper II-14, 1955, pp. 315–319.
[38] J.S. Montes, Undular hydraulic jump – discussion, J. Hyd. Div., ASCE 105 (HY9) (1979) 1208–1211.
[39] N. Rajaratnam, Hydraulic jumps on rough beds, Trans. Engrg. Institute of Canada 11 (A-2) (May 1968) I–VIII.
[40] H.J. Leutheusser, E.J. Schiller, Hydraulic jump in a rough channel, Water Power & Dam Construction 27 (5) (1975) 186–191.
[41] A.T. Troskolanski, Hydrometry: Theory and Practice of Hydraulic Measurements, Pergamon Press, Oxford, UK, 1960, 684 p.
[42] A.J.C. Barré de Saint-Venant, Théorie et Equations Générales du Mouvement Non Permanent des Eaux Courantes, Comptes Rendus des séances de l'Académie des Sciences, Paris, France, Séance 17 July 1871, vol. 73, (1871), pp. 147–154 (in French).
[43] L. Rayleigh, Note on tidal bores, Proc. Royal Soc. of London, Series A containing Papers of a Mathematical and Physical Character 81 (541) (1908) 448–449.
[44] H. Chanson, The Hydraulics of Open Channel Flow: An Introduction, second ed., Butterworth–Heinemann, Oxford, UK, 2004, 630 p.
[45] T.B. Benjamin, M.J. Lighthill, On cnoidal waves and bores, Proc. Roy. Soc. London Ser. A, Math. & Phys. Sci. 224 (1159) (1954) 448–460.

[46] R.A.R. Tricker, Bores, Breakers, Waves and Wakes, American Elsevier Publ. Co., New York, USA, 1965.
[47] D.H. Peregrine, Calculations of the development of an undular bore, J. Fluid Mech. 25 (1966) 321–330.
[48] D.L. Wilkinson, M.L. Banner, Undular bores, in: Proc. 6th Australasian Hyd. and Fluid Mech. Conf., Adelaide, Australia, 1977, pp. 369–373.
[49] A.F. Teles Da Silva, D.H. Peregrine, Nonsteady computations of undular and breaking bores, in: Proc. 22nd Int. Cong. Coastal Eng., vol. 1, ASCE Publ., Delft, The Netherlands, 1990, pp. 1019–1032.
[50] O.C. Zienkiewicz, J.A. Sandover, The undular surge wave, in: Proc. of the 7th IAHR Congress, vol. II, Lisbon, Portugal, paper D25, 1957, pp. D1–11.
[51] J.A. Sandover, P. Holmes, The hydraulic jump in trapezoidal channels, Water Power 14 (Nov. 1962) 445–449.
[52] J. Ponsy, M. Carbonnell, Etude photogrammétrique d'intumescences dans le canal de l'Usine d'Oraison (Basses-Alpes), J. Soc. Française de Photogram. 22 (1966) 18–28.
[53] J. Sander, K. Hutter, On the development of the theory of the solitary wave. A historical essay, Acta Mech. 86 (1991) 111–152.
[54] J.A. Cunge, Undular bores and secondary waves – experiments and hybrid finite-volume modelling, J. Hyd. Res., IAHR 41 (5) (2003) 557–558.
[55] P.A. Madsen, I.A. Svendsen, Turbulent bores and hydraulic jumps, J. Fluid Mech. 129 (1983) 1–25.
[56] J.G. Caputo, Y. Stepanyants, Bore formation, evolution and disintegration into solitons in shallow inhomogeneous channels, Nonlinear Processes in Geophysics 10 (2003) 407–424.
[57] P.A. Madsen, H.J. Simonsen, C.H. Pan, Numerical simulation of tidal bores and hydraulic jumps, Coastal Eng. 52 (5) (2005) 409–433.
[58] G.A. El, R.H.J. Grimshaw, A.M. Kamchatnov, Evolution of solitary waves and undular bores in shallow-water flows over a gradual slope with bottom friction, J. Fluid Mech. 585 (2007) 213–244.
[59] H.H. Yeh, K.M. Mok, On turbulence in bores, Phys. Fluids, Ser. A 2 (5) (1990) 821–828.
[60] H.G. Hornung, C. Willert, S. Turner, The flow field downstream of a hydraulic jump, J. Fluid Mech. 287 (1995) 299–316.
[61] J. Piquet, Turbulent Flows. Models and Physics, Springer, Berlin, Germany, 1999, 761 p.
[62] H. Rouse, T.T. Siao, S. Nagaratnam, Turbulence characteristics of the hydraulic jump, Trans. ASCE 124 (1959) 926–950.
[63] F.J. Resch, H.J. Leutheusser, Reynolds stress measurements in hydraulic jumps, J. Hyd. Res., IAHR 10 (4) (1972) 409–429.
[64] M. Liu, Turbulence structure in hydraulic jumps and vertical slot fischways, in: Ph.D. thesis. Dept. of Civil and Env. Eng., University of Alberta, Edmonton, Canada, 2004, 313 p.
[65] Arrian, Arrian, Harvard University Press, Cambridge, USA, 1976. Translated by P.A. Brunt, 2 volumes.
[66] Quintus Curcius, The History of Alexander, Penguin, New York, 1984. Translated by J. Yardley, 332 p.
[67] B. Kjerfve, H.O. Ferreira, Tidal bores: First ever measurements, Ciência e Cultura (J. Brazilian Assoc. for the Advancement of Science) 45 (2) (March/April 1993) 135–138.
[68] E. Wolanski, D. Williams, S. Spagnol, H. Chanson, Undular tidal bore dynamics in the Daly Estuary, Northern Australia, Estuarine, Coastal and Shelf Science 60 (4) (2004) 629–636.
[69] J.H. Simpson, N.R. Fisher, P. Wiles, Reynolds stress and TKE production in an estuary with a tidal bore, Estuarine, Coastal and Shelf Science 60 (4) (2004) 619–627.
[70] G.H. Darwin, The Tides and Kindred Phenomena in the Solar System, Lectures delivered at the Lowell Institute, Boston, 1897 W.H. Freeman and Co. Publ., London, 1962.
[71] R.N. Moore, Report on the Bore of the Tsien-Tang Kiang, Hydrographic Office, London, 1888.
[72] Z. Dai, C. Zhou, The Qiantang bore, Int. J. Sediment Res. (1) (November 1987) 21–26.
[73] W.N. Beaver, Unexplored New Guinea. A Record of the Travels, Adventures, and Experiences of a Resident Magistrate amongst the Head-Hunting Savages and Cannibals of the Unexplored Interior of New Guinea, Seeley, Service & Co, London, UK, 1920, 320 p.
[74] J.J. Malandain, La Seine au Temps du Mascaret, Le Chasse-Marée, No. 34, 1988, pp. 30–45 (in French).
[75] C. Davies, Tidal River bores. Dissertation in partial fulfilment of B.A. degree, Dept. of Geography, Edge Hill College, University of Lancaster, UK, 1988.
[76] H. Bazin, Recherches Expérimentales sur la Propagation des Ondes. Mémoires présentés par divers savants à l'Académie des Sciences, Paris, France, vol. 19, 1865, pp. 495–644 (in French).
[77] A. Locke, J.M. Hanson, G.J. Klassen, S.M. Richardson, C.I. Aube, The damming of the Petiticodiac River: Species, populations, and habitats lost, Northeastern Naturalist 10 (1) (2003) 39–54.
[78] H. Chanson, Air Bubble Entrainment in Free-Surface Turbulent Shear Flows, Academic Press, London, UK, 1997, 401 p.
[79] H. Chanson, T. Brattberg, Experimental study of the air–water shear flow in a hydraulic jump, Int. J. Multiphase Flow 26 (4) (2000) 583–607.
[80] A.A. Kalinske, J.M. Robertson, Closed conduit flow, Trans. ASCE 108 (1943) 1435–1447.
[81] P. Wisner, Sur le Rôle du Critère de Froude dans l'Etude de l'Entraînement de l'Air par les Courants à Grande Vitesse, in: Proc. 11th IAHR Congress, Leningrad, USSR, paper 1.15, 1965 (in French).
[82] N. Rajaratnam, An experimental study of air entrainment characteristics of the hydraulic jump, J. Inst. Eng. India 42 (7) (March 1962) 247–273.
[83] F.J. Resch, H.J. Leutheusser, Le ressaut hydraulique : mesure de turbulence dans la région diphasique, J. La Houille Blanche (4) (1972) 279–293 (in French).
[84] H. Chanson, Air entrainment in two-dimensional turbulent shear flows with partially developed inflow conditions, Int. J. Multiphase Flow 21 (6) (1995) 1107–1121.
[85] M. Mossa, U. Tolve, Flow visualization in bubbly two-phase hydraulic jump, J. Fluids Eng., ASME 120 (March 1998) 160–165.
[86] F. Murzyn, D. Mouaze, J.R. Chaplin, Optical fibre probe measurements of bubbly flow in hydraulic jumps, Int. J. Multiphase Flow 31 (1) (2005) 141–154.
[87] H. Chanson, Bubbly flow structure in hydraulic jump, Eur. J. Mech. B/Fluids 26 (3) (2007) 367–384. doi:10.1016/j.euromechflu.2006.08.001.
[88] H. Chanson, Dynamic similarity and scale effects affecting air bubble entrainment in hydraulic jumps, in: M. Sommerfield (Ed.), Proc. 6th International Conference on Multiphase Flow ICMF 2007, Leipzig, Germany, July 9–13, 2007, Session 7, Paper S7_Mon_B_S7_Mon_B_3, 11 p. (CD-ROM).
[89] H. Chanson, The Hydraulics of Open Channel Flow: An Introduction, Edward Arnold, London, UK, 1999, 512 p.
[90] I.R. Wood, Air entrainment in free-surface flows, in: IAHR Hydraulic Structures Design Manual, No. 4. Hydraulic Design Considerations, Balkema Publ., Rotterdam, The Netherlands, 1991, p. 149.
[91] F. Murzyn, H. Chanson, Free surface, bubbly flow and turbulence measurements in hydraulic jumps, Report No. CH63/07, Div. of Civil Engineering, The University of Queensland, Brisbane, Australia, July 2007, 116 p.
[92] F. Murzyn, H. Chanson, Experimental assessment of scale effects affecting two-phase flow properties in hydraulic jumps, Exp. Fluids 44 (2008). doi:10.1007/s00348-008-0494-4.
[93] H. Chanson, T. Brattberg, Air entrainment by two-dimensional plunging jets: the impingement region and the very-near flow field, in: Proc. 1998 ASME Fluids Eng. Conf., FEDSM'98, Washington, DC, USA, June 21–25, 1998, Paper FEDSM98-4806, 8 p. (CD-ROM).
[94] P.D. Cummings, H. Chanson, Air entrainment in the developing flow region of plunging jets. Part 1. Theoretical development, J. Fluids Engrg., Trans. ASME 119 (3) (1997) 597–602.
[95] H. Chanson, Hydraulic jumps: Bubbles and bores. in: Proc. 16th Australasian Fluid Mechanics Conference AFMC, Gold Coast, Australia, 2–7 December, Plenary Address, 2007, pp. 39–53 (CD-ROM).